Available online at www.sciencedirect.com
ScienceDirect
Geochimica et Cosmochimica Acta 71 (2007) 4786–4813
Geochimica et Cosmochimica Acta
www.elsevier.com/locate/gca

NanoSIMS isotopic analysis of small presolar grains: Search for Si_3N_4 grains from AGB stars and Al and Ti isotopic compositions of rare presolar SiC grains

Ernst Zinner [a,*], Sachiko Amari [a], Robert Guinness [a,1], Cristine Jennings [b,2], Aaron F. Mertz [a,3], Ann N. Nguyen [a,4], Roberto Gallino [c], Peter Hoppe [d], Maria Lugaro [e], Larry R. Nittler [f], Roy S. Lewis [g]

[a] *Laboratory for Space Sciences and the Physics Department, Washington University, One Brookings Drive, St. Louis, MO 63130, USA*
[b] *Laboratory for Space Sciences and Earth and Planetary Sciences Department, Washington University, One Brookings Drive, St. Louis, MO 63130, USA*
[c] *Dipartimento di Fisica Generale, Università di Torino, Via P. Giuria 1, I-10125 Torino, Italy*
[d] *Max-Planck-Institut für Chemie, Abteilung Partikelchemie, P.O. Box 3060, D-55020 Mainz, Germany*
[e] *Astronomical Institute, University of Utrecht, Postbus 80000, 3508 TA Utrecht, The Netherlands*
[f] *Department of Terrestrial Magnetism, Carnegie Institution of Washington, 5241 Broad Branch Road, NW Washington, DC 20015, USA*
[g] *Chicago Center for Cosmochemistry and Enrico Fermi Institute, University of Chicago, Chicago, IL 60637, USA*

Received 12 January 2007; accepted in revised form 11 July 2007; available online 6 August 2007

Abstract

We report isotopic ratio measurements of small SiC and Si_3N_4 grains, with special emphasis on presolar SiC grains of type Z, and new nucleosynthesis models for $^{26}Al/^{27}Al$ and the Ti isotopic ratios in asymptotic giant branch (AGB) stars. With the NanoSIMS we analyzed 310 SiC grains from Murchison (carbonaceous CM2 chondrite) separate KJB (diameters 0.25–0.45 μm) and 153 SiC grains from KJG (diameters 1.8–3.7 μm), 154 SiC and 23 Si_3N_4 grains from Indarch (enstatite EH4 chondrite) separate IH6 (diameters 0.25–0.65 μm) for their C and N isotopic compositions, 549 SiC and 142 Si_3N_4 grains from IH6 for their C and Si isotopic compositions, 13 SiC grains from Murchison and 66 from Indarch for their Al–Mg compositions, and eight SiC grains from Murchison and 10 from Indarch for their Ti isotopic compositions. One of the original objectives of this effort was to compare isotopic analyses with the NanoSIMS with analyses previously obtained with the Cameca IMS 3f ion microprobe. Many of the Si_3N_4 grains from Indarch have isotopic anomalies but most of these apparently originate from adjacent SiC grains. Only one Si_3N_4 grain, with ^{13}C and ^{14}N excesses, has a likely AGB origin. The C, N, and Si isotopic data show that the percentage of SiC grains of type Y and Z increase with decreasing grain size (from ~1% for grains >2 μm to ~5–7% for grains of 0.5 μm), providing an opportunity for isotopic analyses in these rare grains. Our measurements expand the number of Al–Mg analyses on SiC Z grains from 4 to 23 and the number of Ti analyses on Z grains from 2 to 11. Inferred $^{26}Al/^{27}Al$ ratios of Z grains are in the range found in mainstream and Y grains and do not exceed those predicted by models of AGB nucleosynthesis. Cool bottom processing (CBP) has been invoked to explain the low $^{12}C/^{13}C$ ratios of Z grains, but this process apparently does not lead to increased ^{26}Al production in the parent stars of these grains. This finding is in contrast to presolar oxide grains where CBP is needed to explain their high $^{26}Al/^{27}Al$ ratios. The low $^{46,47,49}Ti/^{48}Ti$ ratios found in Z grains and their correlation with low $^{29}Si/^{28}Si$ ratios extend the trend seen in mainstream

* Corresponding author. Fax: +1 314 935 4083.
E-mail address: ekz@wustl.edu (E. Zinner).
[1] Present address: ESCG/Hamilton Sunstrand, Houston, TX 77058, USA.
[2] Present address: College of Science, Weber State University, Ogden, UT 84408, USA.
[3] Present address: Yale University, New Haven, CT 06520, USA.
[4] Present address: Department of Terrestrial Magnetism, Carnegie Institution of Washington, NW Washington, DC 20015, USA.

0016-7037/$ - see front matter © 2007 Elsevier Ltd. All rights reserved.
doi:10.1016/j.gca.2007.07.012

grains and confirm an origin in low-metallicity AGB stars. The relatively large excesses in ^{30}Si and ^{50}Ti in Z grains are predicted by our models to be the result of increased production of these isotopes by neutron-capture nucleosynthesis in low-metallicity AGB stars. However, the predicted excesses in ^{50}Ti (and ^{49}Ti) are much larger than those found. Even lowering the strength of the ^{13}C pocket cannot solve this discrepancy in a consistent way.
© 2007 Elsevier Ltd. All rights reserved.

1. INTRODUCTION

Primitive meteorites contain presolar grains of stellar origin that can be extracted and studied in the laboratory (Anders and Zinner, 1993; Ott, 1993; Bernatowicz and Zinner, 1997; Zinner, 1998, 2004; Hoppe and Zinner, 2000; Nittler, 2003; Clayton and Nittler, 2004; Lodders and Amari, 2005). Among the presolar grain types identified to date, silicon carbide has been studied in most detail. One reason for this is that SiC is chemically refractory and almost pure separates of SiC can be isolated from meteorites. Furthermore, SiC contains relatively high concentrations of trace elements that can be analyzed for their isotopic compositions in addition to the major elements C and Si. While some isotopic analyses have also been made on collections of many grains (see, e.g., Hoppe and Ott, 1997), most analyses have been made on individual grains by Secondary Ion Mass Spectrometry (SIMS) in the ion microprobe (e.g, Hoppe et al., 1994, 1996a; Huss et al., 1997; Nittler and Alexander, 2003), but also by Resonance Ionization Mass Spectrometry (RIMS) (e.g., Savina et al., 2003) and gas mass spectrometry (Nichols et al., 1995; Heck et al., 2007).

On the basis of their C, N, and Si isotopic compositions, SiC grains have been classified into different subtypes (Hoppe et al., 1994; Hoppe and Ott, 1997). Among these, mainstream grains and grains of type Y and Z are believed to have originated from low-mass (1–3 $M_\odot$) carbon-rich Asymptotic Giant Branch (AGB) stars during their thermally pulsing (TP) phase of evolution. The other SiC grain types apparently come from Type II supernovae, novae and possibly from J-type carbon stars (Nittler, 2003; Zinner, 2004). The most convincing evidence for an AGB origin of mainstream grains comes from the s-process isotopic signatures of heavy elements (see, e.g., Gallino et al., 1997; Hoppe and Ott, 1997; Lugaro et al., 2003a), but the C, N, Al, and Si isotopic ratios are also compatible with such an origin (Hoppe et al., 1994; Huss et al., 1997; Lugaro et al., 1999; Nittler and Alexander, 2003).

Previous measurements of SiC grains (Hoppe et al., 1994, 1996a,b, 1997, 2004; Huss et al., 1997; Nittler and Alexander, 2003; Nittler and Hoppe, 2004) have shown that the abundances of different grain types depend on grain size. In particular, the abundances of Y and Z grains increase with decreasing grain size (Hoppe et al., 1996b, 1997; Zinner et al., 2006b). The NanoSIMS with its high sensitivity and spatial resolution makes it possible to analyze the isotopic ratios of minor and trace elements also in small grains. As a consequence, NanoSIMS analysis of small grains opens the possibility to measure isotopic ratios in rare grains where only a paucity of data exists. Most of the isotopic analyses reported here were made on SiC grains from the SiC-rich Indarch (EH4) separate IH6 (0.25–0.65 μm in diameter), one of the size fractions prepared by Jennings et al. (2002). Like other SiC-rich separates from enstatite chondrites (Stone et al., 1991; Lee et al., 1992; Alexander et al., 1994; Russell et al., 1997; Besmehn and Hoppe, 2001; Besmehn et al., 2001; Lin et al., 2002) the IH6 separate contains a high abundance of silicon nitride (Si_3N_4). In the present work we concentrated on two objectives: (1) investigate the possible stellar sources of Si_3N_4 grains from Indarch and (2) obtain ^{26}Al/^{27}Al and Ti isotopic ratios on the rare grain types A + B, Y and Z.

(1) Silicon nitride grains with supernova (SN) isotopic signatures have previously been identified (Gao et al., 1995; Nittler et al., 1995; Hoppe et al., 1996b; Besmehn and Hoppe, 2001; Lin et al., 2002; Nittler and Alexander, 2003), but the question remained, whether presolar silicon nitride from other stellar sources exists.
(2) Aluminum and Ti isotopic data have previously been obtained on many mainstream grains (Hoppe et al., 1994, 2004; Huss et al., 1997; Alexander and Nittler, 1999), and on A + B and Y grains (Hoppe et al., 1994; Huss et al., 1997; Amari et al., 2001b,c). In contrast, Al isotopic data have only been obtained on four Z grains (Hoppe et al., 1994, 1997; Huss et al., 1997) and Ti isotopic data on two Z grains (Amari et al., 2005). A major objective of the present study was thus to measure Al and Ti isotopic ratios in Z grains.

Silicon carbide grains of type Y and Z are distinguished from the other grain types by their C, N, and Si isotopic compositions (see, e.g., Figs. 1 and 2 of Zinner et al., 2006b). Y grains are defined as having ^{12}C/^{13}C > 100 and Si isotopic ratios that plot to the right of the mainstream correlation line in a Si 3-isotope plot. The latter property and the fact that their ^{14}N/^{15}N > solar (272)[5] distinguish them from X grains, most of which also have ^{12}C/^{13}C > 100. Z grains have, on average, even larger ^{30}Si excesses relative to the mainstream correlation line but have ^{12}C/^{13}C < 100. Most have δ^{29}Si < 0 but a few grains with δ^{29}Si > 0 are also included among Z grains. Nova grain candidates can also have large ^{30}Si excesses but have ^{14}N/^{15}N < solar, whereas Z grains have ^{14}N/^{15}N > solar.

[5] We use the N isotopic ratio of air for solar, although the ratio of 435 measured in Jupiter's atmosphere might be more representative of that of the solar system (Owen et al., 2001).

The percentage of Z grains with diameters larger than 1 μm is ~1.5% of all presolar SiC grains (Nittler and Alexander, 2003; Nittler and Hoppe, 2004) but that of sub-micron grains could be as high as ~4% (Hoppe et al., 1996b, 1997). Whereas mainstream grains are believed to come from AGB stars of solar metallicity, Y grains, which have higher $^{12}C/^{13}C$ ratios, lower $^{29}Si/^{28}Si$ ratios and ^{30}Si excesses compared to mainstream grains, apparently originated from AGB stars of approximately half solar metallicity (Amari et al., 2001b). Hoppe et al. (1997) proposed that Z grains, which have even lower $^{29}Si/^{28}Si$ ratios and larger ^{30}Si excesses, come from AGB stars with approximately one-third solar metallicity (see also Nittler and Alexander, 2003; Zinner et al., 2006b).

Measurements of the Al and Ti isotopic ratios in grains from AGB stars are important because these ratios are affected by different nucleosynthetic processes and such analyses can provide information about AGB nucleosynthesis in addition to that obtained from the C, N, and Si isotopic ratios. Aluminum-26 is produced by proton capture on ^{25}Mg in the H-burning shell (Forestini et al., 1991; Forestini and Charbonnel, 1997; Mowlavi and Meynet, 2000; Karakas and Lattanzio, 2003; Wasserburg et al., 2006) or close to it during extra mixing processes such as cool bottom processing (Wasserburg et al., 1995, 2006; Nollett et al., 2003). In contrast, the Ti isotopes are affected by neutron capture during He burning. Like for the Si isotopes, the nucleosynthetic shifts for the Ti isotopes are comparable to the isotopic variations due to galactic evolution effects. In this sense, Si and Ti are distinct from the heavy elements such as Zr, Mo, and Ba, whose isotopic compositions are completely dominated by AGB nucleosynthesis. In Section 4.1. we provide a short introduction to nucleosynthesis in AGB stars and how it is expected to affect the Al and Ti isotopes in grains from such stars.

Preliminary results of this study have been reported by Amari et al. (2002), Zinner et al. (2003a, 2005a), and Hoppe et al. (2004).

2. EXPERIMENTAL

2.1. Chemical and physical separation

The separation of SiC-rich fractions from the Murchison meteorite have previously been described (Amari et al., 1994; Besmehn and Hoppe, 2003; Nittler and Alexander, 2003). Here, we describe the procedure used for the Indarch EH4 enstatite chondrite. This separation procedure followed the method developed in Chicago (Amari et al., 1994) and essentially consisted of dissolving silicates in hydrofluoric acid and remaining carbon and chromate in perchloric acid. One difference was that the resulting residue did not contain any significant amount of spinel and was therefore not treated with sulfuric acid to remove it.

In more detail, three fragments of Indarch with a total mass of 130 g were crushed with a hammer, rinsed in 20% HCl–80% isopropanol, and treated for 40 min in 3 M HCl at 60 °C to remove surface contamination. The material was then subjected to repeated cycles of alternating treatment with 10 M HF–1 M HCl and 6 M HCl at 50 °C, followed with 6 M HCl–0.6 M H_3BO_3 at 50 °C. Next, the sample went through repeated alternating cycles of 2 M HF–6 M HCl and 3 M HCl–saturated H_3BO_3, was rinsed with 0.1 M HCl, treated once more with 3 M HCl–saturated H_3BO_3, rinsed several times with 0.1 M HCl, finally with methanol, and was dried. The residue of 4.2 g was then repeatedly treated with CS_2 to remove sulfur, and with 0.5 N $Na_2Cr_2O_7 \cdot 2H_2O$–2 N H_2SO_4 for 24 h at 85 °C in order to dissolve kerogen and remove remaining sulfur. Nanodiamonds were removed by colloidal separation at an appropriate pH value. Half of the remaining residue was treated three times with 70% $HClO_4$ for 2 h at the boiling temperature of 210 °C in order to oxidize carbon and remaining organic material as well as dissolve chromate grains. After treatment with NaOH to remove possible tungsten oxides (a small aliquot had been exposed to Na-polytungstate in a failed attempt to separate graphite and had been added back to the residue), the residue was separated into seven size fractions. Separate IH6 comprises grains with diameters between 0.25 and 0.65 μm as determined by SEM measurements. A final 10 M HF–1 M HCl treatment was performed to remove contaminant glass.

Eight of the SiC grains for which we report Ti isotopic compositions and 11 A + B SiC grains for which we report Al–Mg data were obtained from a Murchison SiC separate that was prepared at the MPI Mainz (Besmehn and Hoppe, 2003) according to the standard Chicago procedure.

2.1.1. SIMS analysis

All analyzed grains were deposited on a gold foil from suspension in a propanol–water mixture.

2.1.2. Automatic search with the Cameca IMS 6f at the Carnegie Institution

In order to locate rare grain types, 1300 grains from a Murchison SiC-rich residue prepared at the MPI Mainz (Besmehn and Hoppe, 2003) were automatically analyzed for their C- and Si-isotopic compositions (Nittler and Hoppe, 2005) in the way described by Nittler and Alexander (2003). Eleven A + B grains identified in this way were subsequently analyzed for Mg–Al and four Z, three mainstream, and one Y grain for their Ti-isotopic compositions in the NanoSIMS in Mainz.

2.1.3. Isotopic analysis with the NanoSIMS

All isotopic measurements were made at high enough mass resolving power to eliminate interferences from molecular ions. However, possible isobaric interferences from ^{46}Ca, ^{48}Ca, ^{50}V, and ^{50}Cr with the Ti isotopes could not be eliminated in this way. Carbon and N isotopic ratios were measured in multidetection. Five electron multipliers detected $^{12}C^-$, $^{13}C^-$, $^{12}C^{14}N^-$, $^{12}C^{15}N^-$, and $^{28}Si^-$ ions produced by a Cs^+ beam. During analysis the magnetic field was kept at a constant value under Nuclear Magnetic Resonance (NMR) control. Measurements were done in the so-called grain mode (e.g., Zinner et al., 2003b). In this method candidate grains are identified from a 20 × 20-μm raster image of secondary ions and electrons. To make an isotopic measurement, the primary beam is deflected onto a selected grain and rastered over a small area (typically 0.8 × 0.8 μm).

Synthetic SiC and Si_3N_4 grains were used as C and N isotopic standards. Carbon and Si isotopic ratios were also measured in multidetection grain mode, with the five electron multipliers counting $^{12}C^-$, $^{13}C^-$, $^{28}Si^-$, $^{29}Si^-$, and $^{30}Si^-$ ions. Synthetic SiC and Si_3N_4 grains were used as C and Si isotopic standards.

The Al–Mg and Ti isotopic measurements were made by detecting positive secondary ions produced with an O^- beam. For Al–Mg the ions $^{24}Mg^+$, $^{25}Mg^+$, $^{26}Mg^+$, $^{27}Al^+$, and $^{28}Si^+$ were counted simultaneously in multidetection grain mode. In St. Louis the O^- beam was rastered over a 0.8×0.8 μm area, in Mainz the raster size varied from 1.6 to 3.2 μm. Burma spinel was used as a standard for the Mg isotopic ratios in both laboratories. For the Al/Mg ratio in the SiC grains Burma spinel was used in St. Louis, small Murchison spinel grains were used in Mainz.

The Ti isotopic ratios were measured in the combined detection method, which is a combination of multidetection and magnetic peak jumping (Stadermann et al., 2005). In this method the magnetic field is cycled through a set of values and for each field setting different combinations of isotopes are measured in multidetection. Five Z grains from Indarch were analyzed in St. Louis and four Z grains from Murchison in Mainz. The conditions for these analyses were somewhat different. In St. Louis three field steps were used. In the first step we detected ^{40}Ca, ^{44}Ca, ^{47}Ti, and ^{50}Ti in multipliers 2–5, in the second step ^{28}Si, ^{48}Ti, and ^{51}V in multipliers 1, 4, and 5, in the third step ^{46}Ti, ^{49}Ti, and ^{52}Cr in multipliers 3, 4, and 5. Calcium, V, and Cr were measured to make corrections for isobaric interferences of these elements to Ti, which were very small for ^{46}Ca, ^{48}Ca, and ^{50}V but reached 30% for ^{50}Cr in grain Mur-i11B-179-1. We assumed a normal $^{50}Cr/^{52}Cr$ ratios for the ^{50}Cr correction because we do not know whether the Cr is indigenous to the grains or contamination. If Cr is indigenous, it is expected to be isotopically anomalous and AGB models predict depletions in ^{50}Cr relative to ^{52}Cr. The predicted maximum depletions are 24‰, 58‰, and 115‰ in stars with metallicities $Z = 0.02$ (solar), $Z = 0.006$ and 0.003, respectively. If we apply these depletions to the corrections made for mainstream, Y, and Z grains, the maximum errors (Y and Z grains are more likely from stars with $Z = 0.01$ and 0.006) made in the ^{50}Cr correction are 11‰ for grain Mur11B-123-4 and 12‰ for grain Mur11B-476-6. All other errors are smaller than 10‰. These maximum errors are much smaller than the experimental uncertainties on the $^{50}Ti/^{48}Ti$ ratio. Terrestrial perovskite was used as isotopic standard. In Mainz two field steps were used. In the first we detected ^{28}Si, ^{46}Ti, ^{48}Ti, ^{50}Ti, and ^{52}Cr, in the second ^{47}Ti, ^{49}Ti, ^{51}V, and ^{53}Cr. A Ti-rich large grain from Murchison, NBS steel and Ti metal were used as standards. Because no Ca isotopes were measured, no corrections for ^{46}Ca and ^{48}Ca interferences were made, but the St. Louis results and earlier measurements (Amari et al., 1995, 2000) indicate that ^{46}Ca and ^{48}Ca interferences are <1‰ and <3‰, respectively.

All errors given in the tables include the analytical uncertainties for individual grain measurements and the variations in the repeated measurements on the standards.

3. C, N, AND SI ISOTOPIC RATIOS OF SMALL SIC GRAINS AND THE SEARCH FOR SILICON NITRIDE GRAINS FROM AGB STARS

A survey of all the C, N, and Si isotopic measurements performed in this study is given in Table 1 and the results are plotted in Figs. 1–4. In addition to grains from the Indarch IH6 separate, we also analyzed grains from the SiC-rich separates KJB (diameters 0.25–0.45 μm) and KJG (diameters 1.8–3.7 μm) (Amari et al., 1994). The reason was to compare isotopic measurements with the NanoSIMS with those previously made with the Cameca IMS 3f ion microprobe (Hoppe et al., 1994, 1996b). Table 1 shows the classification of the analyzed grains into different types. Since the identification of Z grains requires knowledge of the Si isotopic compositions, C and N isotopic measurements can only identify mostly mainstream (which overlap with Z grains), A + B ($^{12}C/^{13}C < 10$), X ($^{14}N/^{15}N < 250$ and $^{12}C/^{13}C > 5$) and Y ($^{12}C/^{13}C > 100$) grains (see Fig. 1). One IH6 grain with very low $^{12}C/^{13}C$ and $^{14}N/^{15}N$ ratios (labeled N/SN? In Fig. 1b) is possibly a nova grain but could have a SN origin instead (Nittler and Hoppe, 2005). The abundances of different grain types of this study are compared to those of previous studies in Table 2. One obvious observation to be made from this comparison is that the abundance of Y and Z grains increases with decreasing grain size. This fact has previously been noted by Hoppe et al. (1996b), who in KJE (grain size 0.5–1.9 μm) found a Z grain abundance of 2.8%. In a subsequent study, an abundance of 1.8% was found (Hoppe et al., 1997). The abundance of Y grains in the KJG separate seems to fall outside of this trend (Table 2) but it is based on only seven grains and could be the result of statistical fluctuation.

During the C and N isotopic analyses of IH6 grains we found 23 Si_3N_4 grains (Figs. 1 and 2). Although there is a range of Si^-/C^- ratios among grains, we define grains with $^{28}Si^-/^{12}C^- > 4$ as Si_3N_4 (Fig. 2c). These grains have also, on average, higher $^{12}C^{14}N^-/^{12}C^-$ ratios than SiC grains. Their identity as Si_3N_4 has also been confirmed by SEM-EDX analysis. It is not certain that the number of 23 Si_3N_4 grains among 177 analyzed IH6 grains (cf. Table 1) represents their true abundance. The reason is that grains to be analyzed for their isotopic ratios were selected from $^{12}C^-$, $^{28}Si^-$, and secondary electron images and dim grains in the $^{12}C^-$ images might not have been analyzed. In contrast to the Indarch IH6 separate, no Si_3N_4 grains were detected among the Murchison KJG and KJB separates (Fig. 2a and b). Presolar Si_3N_4 grains have previously been found (Nittler et al., 1995; Hoppe et al., 1996b; Besmehn and Hoppe, 2001; Lin et al., 2002). These grains have isotopic signatures similar to those of SiC X grains and have a SN origin. They are extremely rare and their abundance relative to all SiC grains is only ~0.05%. Nittler and Alexander (2003) reported a higher abundance (~0.1%) for a Murchison sample prepared by a different chemical procedure, implying that Si_3N_4 is more easily destroyed by harsh chemical treatments than SiC. The C and N isotopic ratios of such grains are plotted in Fig. 1d. These ratios are quite different from those of the IH6 silicon nitride grains

Table 1
Grain types of presolar SiC identified by C–N and C–Si analysis of SiC separates from Indarch and Murchison

Type	Separates					
	IH6 (grains)	IH6 (%)	KJB (grains)	KJB (%)	KJG (grains)	KJG (%)
C–N analyses						
Mainstream + Z	138	89.6	268	86.5	131	85.6
A + B	8	5.2	20	6.5	12	7.8
X	2	1.3	2	0.6	1	0.7
Y	6	3.9	20	6.5	9	5.9
Total	154	100	310	100	153	100
C–Si analyses						
Mainstream	437	79.6				
A + B	27	4.9				
X	8	1.5				
Y	35	6.4				
Z	42	7.6				
Total	549	100				

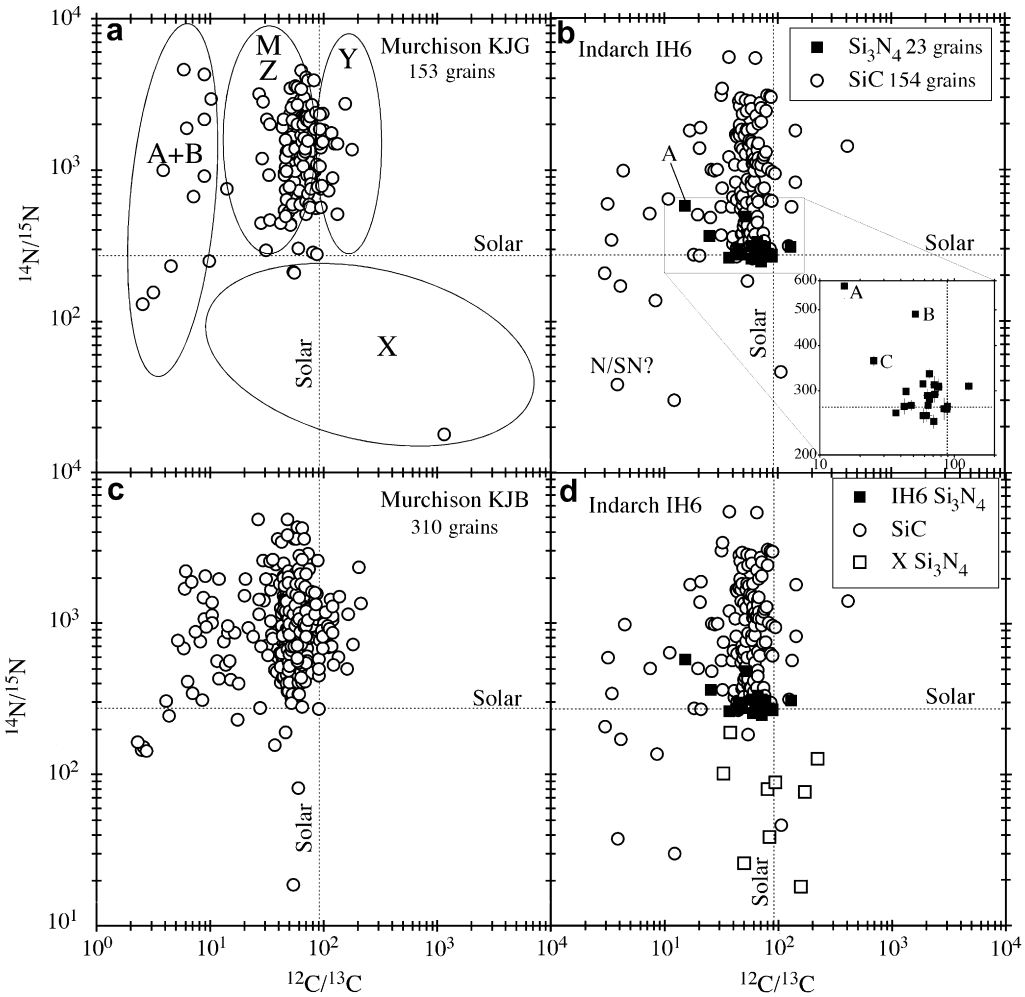

Fig. 1. Nitrogen versus C isotopic ratio plots of presolar SiC grains from the SiC-rich separates Murchison KJG and KJB, and Indarch IH6. Also plotted in (b) and (d) are the isotopic ratios of silicon nitride grains from IH6. In (a) we indicate the approximate ranges of the different types of presolar SiC. In the N vs. C plot the ranges of the mainstream (M) and Z grains overlap, but they are distinct in their Si isotopic ratios (see Fig. 7). The inset in (b) shows only the silicon nitride grains. In (d) we also plotted the N and C isotopic ratios of previously identified X type silicon nitride grains (Nittler et al., 1995; Hoppe et al., 1996b; Besmehn and Hoppe, 2001; Lin et al., 2002).

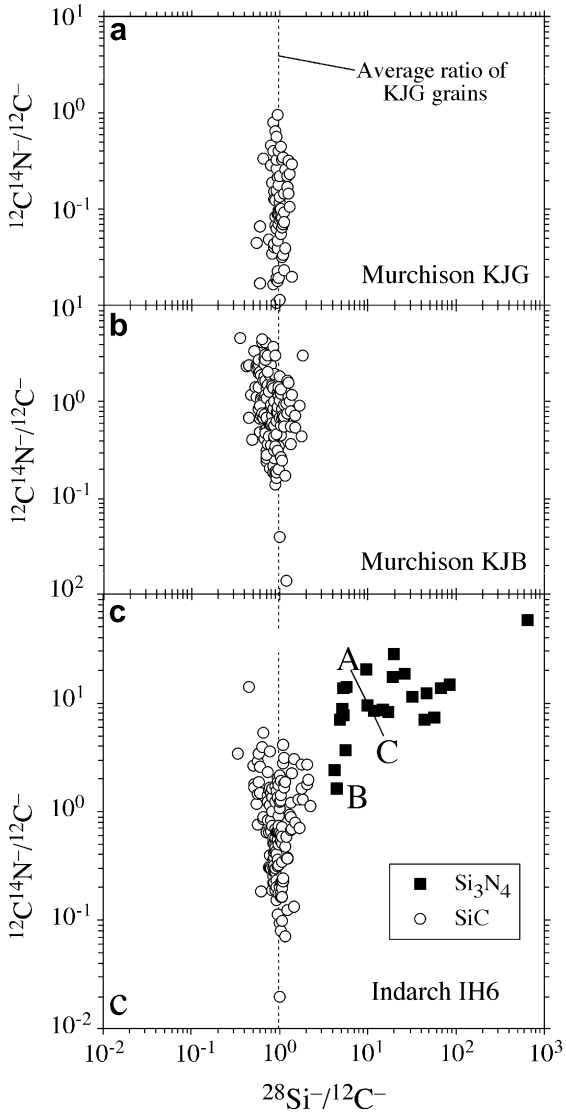

Fig. 2. The ion ratios $^{12}C^{14}N^-/^{12}C^-$ and $^{28}Si^-/^{12}C^-$ determined in the NanoSIMS for SiC and Si_3N_4 grains from the separates Murchison KJG (a) and KJB, (b) and Indarch IH6 (c) are plotted against one another. The $^{28}Si^-/^{12}C^-$ ratio is used to distinguish between SiC and Si_3N_4 grains. The broadening of this ratio in KJB and IH6 SiC grains is probably due to contamination with carbon-rich material and for IH6 with small adjacent Si_3N_4 grains. $^{12}C^{14}N^-/^{12}C^-$ ratios are, on average, much higher in KJB and IH6 than in KJG grains, indicating higher intrinsic N concentrations in smaller grains.

(Fig. 1b and d). However, most IH6 silicon nitride grains are still anomalous and some compositions overlap with those of mainstream SiC grains. Thus the question arises whether some of the Si_3N_4 grains could have an origin in C-rich AGB stars, believed to be the source of mainstream grains.

It has previously been found that enstatite chondrites contain much higher abundances of Si_3N_4 grains than carbonaceous chondrites (Stone et al., 1991; Lee et al., 1992; Alexander et al., 1994; Besmehn and Hoppe, 2001; Besmehn et al., 2001; Lin et al., 2002). Most of these grains have isotopically normal compositions and apparently formed by exsolution from host phases (Alexander et al., 1994). Carbon isotopic anomalies in a few of these grains have been explained by adjacent small presolar SiC grains (Alexander et al., 1994). This could definitely also be the case for the IH6 grains, and SiC grains adjacent to isotopically normal Si_3N_4 grains provide the most likely explanation for the measured C and N isotopic compositions of most Si_3N_4 grains. Even grain B, whose C and N isotopic ratios are quite anomalous (inset of Fig. 1b), can be explained this way. As can be seen in Fig. 2c, the $^{12}C^{14}N^-/^{12}C^-$ ratio of this grain is in the range of ratios for SiC grains. The situation is different for grains A and C. The $^{12}C^{14}N^-/^{12}C^-$ ratios of these grains are considerably higher than those of SiC grains, indicating that the CN^- signal from these grains mainly comes from Si_3N_4. If the CN^- signal from the Si_3N_4 is at least three times that from adjacent SiC grains, as indicated by the $^{12}C^{14}N^-/^{12}C^-$ ratios (Fig. 2c), then contamination with SiC grains having pure ^{14}N could explain the $^{14}N/^{15}N$ ratio of grain C but not that of grain A. The problem with this argument is that the $^{12}C^{14}N^-/^{12}C^-$ ratio is not a simple measure for the N content because it depends also on the C content of a phase. However, we do not know the C content of the Si_3N_4 and the N content of adjacent SiC grains and therefore do not know how much of the CN^- signal comes from either grain type. Thus, while it is very plausible that grain A is indeed a presolar Si_3N_4 grain with an isotopic signature indicating an AGB origin, we cannot obtain absolute proof of this hypothesis. It could be that the adjacent SiC has a higher N content than all the other measured SiC grains and a high $^{14}N/^{15}N$ ratio. Of 154 IH6 and 310 KJB SiC grains, not one has the required high $^{12}C^{14}N^-/^{12}C^-$ ratio of greater than 5 to explain the $^{14}N/^{15}N$ ratio of 581 ± 14 of grain A, which requires approximately equal contributions to the CN^- signal from SiC (with essentially pure ^{14}N) and Si_3N_4 (with isotopically normal N.) It is a conservative estimate that the probability that the N isotopic composition of this Si_3N_4 grain is explained by adjacent SiC grains is less than 1%.

We also measured C and Si isotopic ratios in SiC and Si_3N_4 grains from the IH6 separate. The results are plotted in Figs. 3 and 4. The abundance of Si_3N_4, 142 out of 690 analyzed grains, is higher than that in the C–N analyses, 23 out of 177, but this time we were more interested in obtaining data on Si_3N_4 grains and relaxed the Si/C condition (see below). Again, the C isotopic ratios of the Si_3N_4 grains span a large range and are most likely due to adjacent SiC grains (Fig. 4). In contrast, the Si isotopic ratios are rather normal, completely different from those of the SiC grains (Figs. 3 and 4). The exception is one grain with the isotopic signature of a SNII grain, similar to the isotopic signature of 7 SiC X grains from this study and previously identified presolar Si_3N_4 grains with the "X-type" signature (Fig. 3a). Most other Si_3N_4 grains plot close to the origin in a 3-isotope δ-value plot (Fig. 3b and c). Some of them deviate from the normal isotopic composition by more than 2σ but it is difficult to ascertain that they are isotopically anomalous. The reason is, again, that adjacent SiC grains could shift the measured Si isotopic ratios away

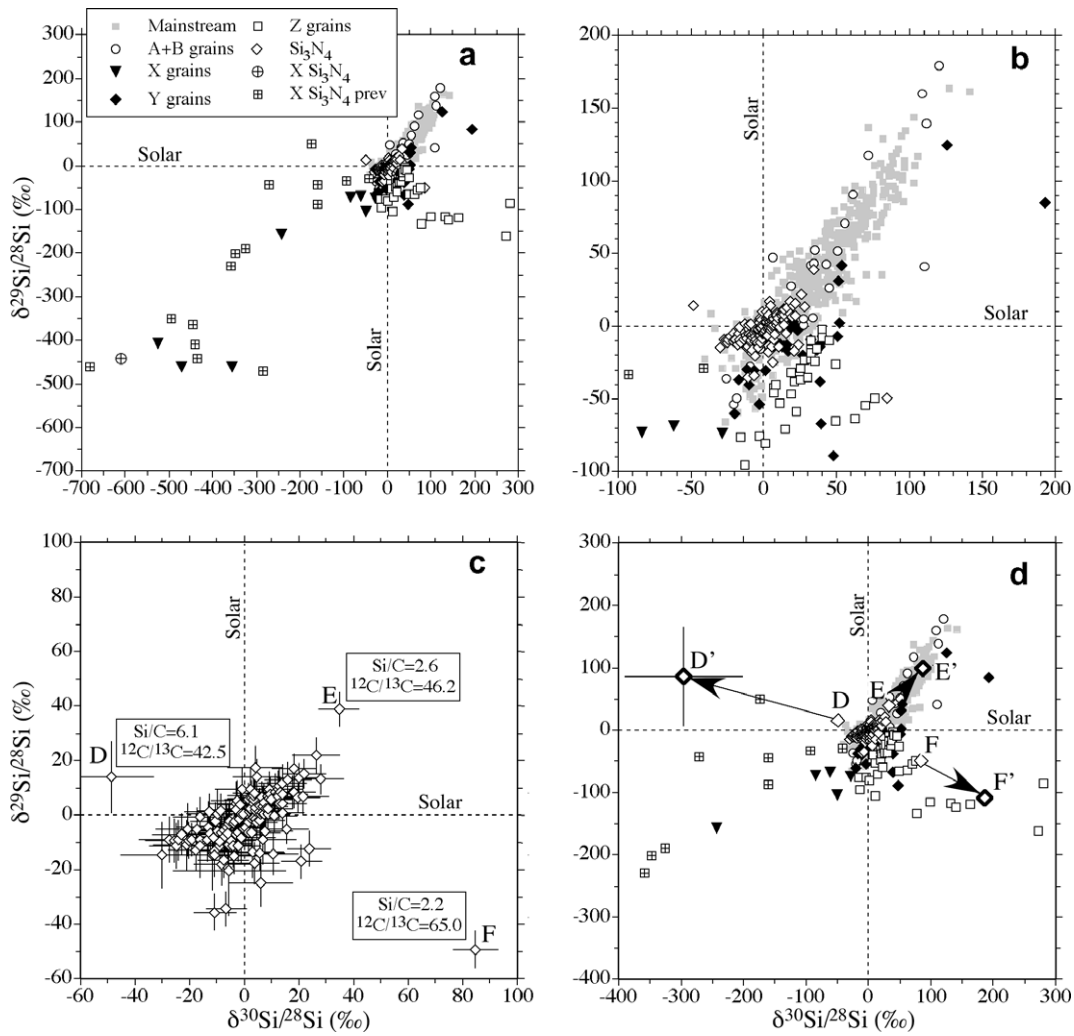

Fig. 3. Silicon isotopic ratios measured in SiC and Si_3N_4 grains from the Indarch separate IH6. The Si ratios are plotted as δ-values, deviations from the solar (=terrestrial) ratios in permil (‰). Symbols for different grain types are given in (a). In (a) and (b) we also plot the Si isotopic ratios of X type Si_3N_4 grains from previous measurements (Nittler et al., 1995; Hoppe et al., 1996b; Besmehn and Hoppe, 2001; Lin et al., 2002). (c) The isotopic ratios of Si_3N_4 grains from Indarch IH6. Three grains with anomalous compositions are indicated. Graph (d) shows the inferred Si isotopic ratios of SiC grains if we assume that their admixture is responsible for the compositions of the three anomalous grains. See text for discussion.

from normal. We looked at this possibility in the case of three Si_3N_4 grains, D, E, and F, which plot away from the bunch of the other grains (Fig. 3c). Since we know the Si/C ratio of these grains (we relaxed the conditions applied for the C–N analyses and considered grains with Si/C as low as 2 to be Si_3N_4) we can calculate the Si isotopic ratios of SiC grains that, if analyzed together with isotopically normal Si_3N_4 grains without any C, would result in the measured ratios. The ratios calculated in this way for the assumed SiC grains are plotted in Fig. 3d. The complementary ratios for grain D are similar to ratios previously obtained for a few X grains, the ratios for grain E correspond to those of mainstream SiC grains, and the ratios for grain F lie in the middle of the region occupied by type Z SiC grains. Thus, from the Si isotopic ratios of Si_3N_4 grains we do not have incontrovertible evidence that any of these grains had an origin in AGB stars. As has previously been concluded (Alexander et al., 1994; Russell et al., 1997), almost all of them must have a solar-system origin.

The best candidate for a Si_3N_4 grain from an AGB star is still grain A with the high $^{14}N/^{15}N$ ratio (Fig. 1b). Silicon nitride is not likely to form as a primary condensate in the envelope of AGB stars. It could form as a reaction product of previously condensed SiC and N_2 gas according to

$$3SiC\ (solid) + 2N_2\ (gas) = Si_3N_4\ (solid) + 3C\ (solid),$$

however such a reaction would require a high partial pressure of N_2. Given the fact that we have only tenuous evidence for Si_3N_4 from AGB stars, we are not going to pursue this question. However, we should mention that Clément et al. (2005) reported the spectroscopic identification of S_3N_4 (in addition to SiC) in circumstellar dust shells of several extreme carbon stars (carbon stars with very thick envelopes).

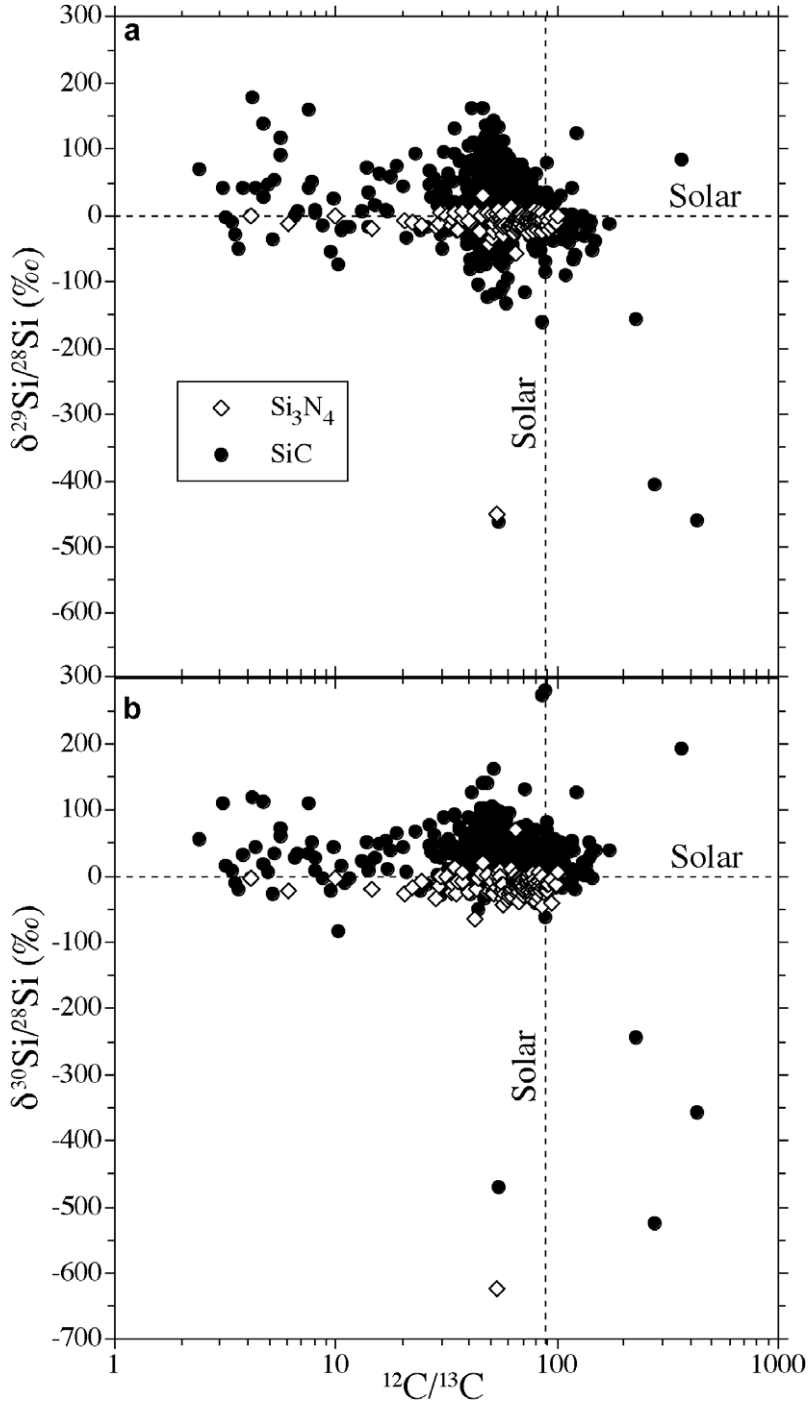

Fig. 4. The Si isotopic ratios of SiC and Si_3N_4 grains from the Indarch separate IH6 are plotted against their C isotopic ratios. Whereas the C isotopic ratios of Si_3N_4 grains cover almost the same range as those of SiC grains, their Si isotopic ratios are close to normal, indicating that adjacent SiC grains are responsible for the C isotopic ratios of the Si_3N_4 grains.

4. ALUMINUM AND TI ISOTOPIC RATIOS OF RARE TYPES OF SIC GRAINS

Before discussing the Al and Ti isotopic data in Z grains we provide a short survey of the nucleosynthetic processes occurring in AGB stars.

4.1. Nucleosynthesis in AGB stars

The Al and Ti isotopic ratios measured in the grains are compared to theoretical predictions for the envelope composition of AGB stars of different mass, metallicity, mass loss, and strength of ^{13}C pocket. During the thermally pulsing

Table 2
Abundances[a] of SiC grain types in different SiC separates

Separate:	IH6[b]	KJB	KJC	KJE[c]	KJG	KJG[d]	KJH[d]	Org	Mur-1	Mur-2
Reference[e]:	This work		Hoppe98-00	Hoppe96	This work	Hoppe94		Huss97	Nittler03	Nittler04
Grain size[f]:	0.25–0.65 μm	0.25–0.45 μm	0.3–0.9 μm	0.5–1.9 μm	1.8–3.7 μm	1.8–3.7 μm	3–6 μm	1.6–6 μm	0.5–1.7 μm	
A + B	4.9	6.2	3.3	6.4	7.8	5.6	6.1	7.1	2.8	4.0
X	1.5	0.6	1.2	1.8	0.7	1.0		0.7	1.2	1.0
Y	6.4	6.5	6.5	2.3	5.9	3.9	1.6	2.9	1.5	1.7
Z	7.6		4.3	2.8				2.1	1.4	1.3
Number[g]	548	310	235	849	153	180	506	140	3343	1150

[a] Abundances are in %.
[b] Abundances based on C–Si analysis.
[c] From Table 2. A total of 396 grains were analyzed for Si in addition to C and N.
[d] In part based on C analysis only.
[e] Hoppe98-00: Hoppe et al. (1994), Hoppe et al. (1997), Hoppe and Zinner (2000) and the grain database at http://presolar.wustl.edu/~pgd/; Hoppe96: Hoppe et al. (1996a); Hoppe94: Hoppe et al. (1994); Huss97: Huss et al. (1997); Nittler03: Nittler and Alexander (2003); Nittler04: Nittler and Hoppe (2004).
[f] There is no uniformly accepted way to report grain sizes. Amari et al. (1994) give mass-weighted averages, which shifts the values toward larger values compared to un-weighted averages. Here, we recalculated 90% ranges (omitting the top and bottom 5%) in size as determined from SEM measurements. IH6 and KJB: present work; KJC, grain database at http://presolar.wustl.edu/~pgd/; KJE: Hoppe et al. (1996a), Appendices); KJG and KJH: Hoppe et al. (1994, Fig. 2); Org: Huss et al. (1997, Table 1); and Mur-1: Nittler and Alexander (2003, Fig. 6). For grain sizes see also the grain database at http://presolar.wustl.edu/~pgd/.
[g] Total number of grains analyzed in the study.

phase of AGB stars nucleosynthesis takes place in a narrow (in mass) region consisting of the H- and He-burning shells and the He intershell, on top of the degenerate C-O core (for details see, e.g., Busso et al., 1999; Lattanzio and Forestini, 1999; Goriely and Mowlavi, 2000; Straniero et al., 2006). Aluminum-26 is produced in the H-burning shell by proton capture on ^{25}Mg and destroyed by neutron capture during recurrent thermal pulses (Forestini et al., 1991; Forestini and Charbonnel, 1997; Mowlavi and Meynet, 2000; Karakas and Lattanzio, 2003; Wasserburg et al., 2006). During the third dredge-up (TDU), which occurs after thermal pulses, the convective envelope dips into layers where H burning, partial He burning in the convective thermal pulse, and neutron capture had taken place and mixes ^{26}Al into the whole envelope and to the surface of the star. Also mixed up by TDU are nuclei modified by neutron capture reactions and ^{12}C produced by the triple-alpha reaction. Dredge-up of ^{12}C increases the C/O (and ^{12}C/^{13}C) ratio of the envelope until the originally O-rich (O > C) star becomes C-rich (C > O) and turns into a carbon star. A C-rich envelope is needed to condense SiC grains in the stellar wind.

It should be noted that theoretical estimates of the ^{26}Al abundance at the surface of AGB stars are very much hampered by the large uncertainty in the ^{26}Al(p,γ)^{27}Si reaction rate, which ranges up to three orders of magnitude (Angulo et al., The NACRE Collaboration, 1999; Iliadis et al., 2001). This results in a two-orders-of-magnitude uncertainty in the computed ^{26}Al/^{27}Al ratio in the envelope, which can be as low as 10^{-5} if the current upper limit for the ^{26}Al(p,γ)^{27}Si reaction rate is used. However, the grain data clearly indicate that the lower theoretical values in the ^{26}Al/^{27}Al ratio cannot hold, limiting the range of uncertainty in the ^{26}Al(p,γ)^{27}Si reaction rate.

The Ti isotopes are affected by neutron capture. In AGB stars there are two distinct reactions that provide neutrons in the He intershell: ^{13}C(α,n)^{16}O and ^{22}Ne(α,n)^{25}Mg. The first reaction occurs under radiative conditions between thermal pulses (Straniero et al., 1997) and produces neutrons with a low density ($\leqslant 10^7$ n cm^{-3}) for a long time. The second reaction occurs during the convective thermal pulse, partial He burning under quasi-explosive conditions, when two α-captures produce large amounts of ^{22}Ne from ^{14}N left from H burning in the CNO cycle. The resulting neutron bursts have a much higher neutron density ($\geqslant 10^{10}$ n cm^{-3}) but last a shorter time and produce a smaller total fluence than those from the ^{13}C source. As is ^{26}Al, the products of neutron capture reactions are mixed to the stellar surface by the TDU. In contrast to Si, whose isotopes are mostly affected by the neutrons from the ^{22}Ne source, the Ti isotopes, mostly ^{50}Ti, are also affected by the neutrons from the ^{13}C source (Lugaro et al., 1999; Zinner et al., 2006b). These neutrons are also responsible for the production of the heavy elements via the *s*-process (Gallino et al., 1998; Lugaro et al., 2003a). The processes responsible for the formation of a layer rich in ^{13}C, the so-called ^{13}C pocket, are still not well understood. Possible mechanisms have been discussed by various authors (Freytag et al., 1996; Herwig et al., 1997, 2003; Busso et al., 1999; Denissenkov and Tout, 2003; Lugaro et al., 2003b; Siess et al., 2004; Herwig, 2005; Lattanzio and Lugaro, 2005; Straniero et al., 2006) and we ask the reader to consult these references.

In our AGB nucleosynthesis models the strength of the ^{13}C pocket, i.e., the amount of ^{13}C and thus the total neutron fluence delivered by it, is essentially a free parameter. However, it is constrained by the elemental and isotopic abundances of the heavy elements in the solar system and in presolar grains from AGB stars. The models consider a range of pocket strengths relative to the "standard (ST) pocket", which best reproduces the s-process element abundances in the solar system (Gallino et al., 1997, 1998; Lugaro et al., 2003a). Recent RIMS measurements of the

isotopic ratios of Zr, Mo, and Ba (Barzyk et al., submitted for publication) and NanoSIMS measurements of Ba (Marhas et al., in press) in individual mainstream SiC grains indicate that the ^{13}C pocket strength required for these grains is restricted to a narrow range (a factor of approximately two) around the ST strength. The same range of ^{13}C pocket strengths has been obtained by comparing spectroscopic observations of heavy elements in AGB star with stellar population synthesis models including the *s* process (Bonacic Marinovic et al., in press).

Here, we give only a short summary of the AGB nucleosynthesis code used for making theoretical predictions and refer for details to the existing literature (Gallino et al., 1998; Lugaro et al., 2003a, 2004; Straniero et al., 2006; Zinner et al., 2006b). The nucleosynthesis models use a postprocessing code that computes α and neutron capture in the He-burning shell and He intershell and proton capture in the H shell, employing a large nuclear network involving more than 400 nuclides (Gallino et al., 1998). Stellar structure parameters needed as input for the postprocessing code are provided by the results of the Frascati Raphson Newton Evolutionary Code (FRANEC, Straniero et al., 1997). For AGB stars with masses 1.5 and 2 $M_\odot$ we used analytical formulae that were obtained by interpolating between a large number of FRANEC models (Straniero et al., 2003, 2006; Zinner et al., 2006b). For the 3 and 5 $M_\odot$ models we used the direct results of FRANEC. Different stellar parameters considered include mass, metallicity, and mass loss during the AGB phase. The mass loss was obtained following the prescription of Reimers (1975)

$$dM/dt(M_\odot\ yr^{-1}) = 1.34 \times 10^{-5}\eta L^{3/2}/(MT_{eff}^2)$$

where M and L are stellar mass and luminosity in solar units, T_{eff} the effective temperature in K and η is a parameter for the mass loss. The effect of mass, metallicity and mass loss on the dredged-up mass and the maximum temperature in the convective zone of consecutive thermal pulses are shown in Zinner et al. (2006b).

The stellar structure models and the derived analytical formulae assume the elemental and isotopic abundances given by Anders and Grevesse (1989) for the solar composition. In contrast, the postprocessing code uses the new solar abundances for C and O (Allende Prieto et al., 2001, 2002; Asplund et al., 2005). These abundances are almost a factor of two lower than the Anders and Grevesse abundances. The major consequence is that, because these abundances are lower and the C/O ratio higher than the old values, C-stars can form more easily and the final C/O ratios at the end of the TP-AGB phase are approximately a factor of two higher. However, the new solar abundances do not affect the predicted abundances and isotopic compositions of elements other than C and O. We note that the solar abundance of the CNO elements is still a contentious issue (see, e.g., Piersanti et al., 2007). While some recent spectroscopic measurements (Socas-Navarro and Norton, 2007) support the low O abundance of Asplund et al. (2005), other measurements (Landi et al., 2007) and especially data on solar oscillations (Chaplin et al., submitted for publication) support a metallicity of close to $Z = 0.02$, consistent with the Anders and Grevesse (1989) value.

For models with lower-than-solar metallicities, the isotopic ratios of elements of interest (Mg, Si, Ti) were calculated by assuming that the abundances of all isotopes except those of the alpha nuclei ^{24}Mg, ^{28}Si, and ^{48}Ti scale with the Fe abundance. The α nuclei, on the other hand, were assumed to be enhanced according to the enhancements observed in thin- and thick-disk stars (Reddy et al., 2003; Bensby et al., 2005; Zinner et al., 2005b; cf. also Zinner et al., 2006b). For Si and Ti we fitted the data points of Reddy et al. (2003) in their Figs. 9 and 10 to straight lines in the [Si/Fe] and [Ti/Fe] versus [Fe/H] plots and shifted the fit so that the lines pass through [S/Fe] = [Ti/Fe] = 0 at the solar metallicity [Fe/H] = 0. In this way we obtain [Si/Fe] = −0.10 × [Fe/H] and [Ti/Fe] = −0.25 × [Fe/H]. This results in ^{28}Si excesses of 12.8% and 20.9% at the metallicities $Z = 0.006$ and 0.003 (corresponding to [Fe/H] values of −0.52 and −0.82) and in $\delta^{29,30}$Si/^{28}Si values of −113‰ and −173‰. For Ti the ^{48}Ti excesses are 35.1% and 60.9% at these metallicities, resulting in $\delta^{46,47,49,50}$Ti/^{48}Ti values of −260‰ and −378‰.

For computing the Si isotopic ratios we used the neutron capture cross-sections given by Guber et al. (2003) rather than those given by Bao et al. (2000). Zinner et al. (2006b) give these different cross-sections (their Table 2) and show their effect on the predicted evolution of the Si isotopic ratios in the envelope of AGB stars. These authors conclude that the Guber et al. cross-sections best explain the Si isotopic ratios of mainstream, Y, and Z grains. The Maxwellian averaged cross-sections (MACSs) of the Ti isotopes recommended by Bao et al. (2000) are at 30 keV in mb: ^{46}Ti 26.8 ± 3.2; ^{47}Ti 64.4 ± 7.7; ^{48}Ti 31.8 ± 5.1; ^{49}Ti 22.1 ± 2.1; ^{50}Ti 3.6 ± 0.4. The uncertainties in the cross-sections result in uncertainties in the predicted isotopic shifts in the envelope of AGB stars. In order to estimate the uncertainties in the shifts we calculated models where we changed the cross-section of a given Ti isotope at a time by 10%. From the results we can estimate the most likely uncertainties in the isotopic shifts. For a 1.5 $M_\odot$ AGB star with metallicity $Z = 0.02$ (solar) the uncertainties on the final isotopic shifts at the end of the TP-AGB phase (expressed as δ-values) are 11.2%, 26.1%, 10.2%, and 4.7% for δ^{46}Ti/^{48}Ti, δ^{47}Ti/^{48}Ti, δ^{49}Ti/^{48}Ti, and δ^{50}Ti/^{48}Ti values, respectively. Because the neutron-magic ^{50}Ti nucleus has the lowest cross-section, the δ^{50}Ti/^{48}Ti value is least affected by uncertainties in the cross-sections. Estimated relative uncertainties are similar for other models with different masses and metallicities. We want to point out that uncertainties in the predicted shifts due to cross-section uncertainties for a given model are much smaller than the variations among models with different masses, metallicities, and strength of the ^{13}C pocket (see discussion in Section 4.3.2).

4.2. Aluminum isotopic ratios of presolar SiC grains

We measured the Al–Mg system in 14 A + B grains, 15 Y grains, two X grains, 17 Z grains and 18 mainstream grains from Indarch separate IH6 as well as in 11 A + B grains and two Z grains from Murchison (Table 3). The measurements on Z grains expanded the previous data on four grains (Hoppe et al., 1997; Huss et al., 1997)

Table 3
Carbon, Si, and inferred Al isotopic ratios of SiC grains from Indarch and Murchison

Type	Meteorite	Grain	$^{12}C/^{13}C \pm 1\sigma$	$\delta^{29}Si/^{28}Si \pm 1\sigma$ (‰)	$\delta^{30}Si/^{28}Si \pm 1\sigma$ (‰)	$^{26}Al/^{27}Al \pm 1\sigma$ ($\times 10^4$
A + B	Indarch	Feb-25-17-12	7.51 ± 0.16	43 ± 5	35 ± 5	28.7 ± 1.7
		Feb-25-21-8	7.63 ± 0.13	160 ± 6	109 ± 6	18.5 ± 1.5
		Feb-25-7-13	3.53 ± 0.05	−28 ± 5	−9 ± 5	8.5 ± 1.5
		Feb-25-7-5	5.63 ± 0.01	91 ± 6	62 ± 6	13.9 ± 0.8
		Feb-25-9-2	3.36 ± 0.05	−10 ± 5	8 ± 5	114.4 ± 3.4
		Feb-25-9-6	5.55 ± 0.07	118 ± 7	72 ± 8	38.6 ± 4.6
		Oct-16-2-6	3.20 ± 0.03	−3 ± 7	16 ± 9	15.6 ± 0.3
		Oct-16-4-10	7.80 ± 0.09	52 ± 7	51 ± 9	4.0 ± 0.7
		Oct-16-4-21	8.70 ± 0.14	−16 ± 7	−2 ± 10	7.8 ± 1.0
		Oct-17-10-23	3.10 ± 0.12	41 ± 5	110 ± 8	175.7 ± 9.8
		Oct-17-15-1	4.30 ± 0.06	43 ± 5	43 ± 8	23.2 ± 4.4
		Oct-17-16-23	4.70 ± 0.08	139 ± 6	112 ± 9	11.6 ± 1.9
		Oct-17-8-18	3.80 ± 0.04	42 ± 6	32 ± 8	31.2 ± 4.1
		IH6-15-11	9.82 ± 0.11	26 ± 6	45 ± 7	6.2 ± 1.0
	Murchison	Muri11B-160-1	3.73 ± 0.04	107 ± 8	63 ± 15	22.6 ± 3.2
		Muri11B-181-3	9.18 ± 0.20	47 ± 10	69 ± 16	8.2 ± 0.6
		Muri11B-184-1	3.69 ± 0.05	13 ± 9	38 ± 16	46.1 ± 1.8
		Muri11B-23-3	4.88 ± 0.22	98 ± 14	81 ± 20	2.6 ± 1.0
		Muri11B-275-1	3.00 ± 0.03	4 ± 8	52 ± 15	20.4 ± 8.4
		Muri11B-287-3	4.36 ± 0.08	−22 ± 8	4 ± 15	58.3 ± 2.5
		Muri11B-326-1	2.46 ± 0.03	−20 ± 9	−3 ± 15	47.5 ± 3.3
		Muri11B-327-1	4.19 ± 0.06	84 ± 9	57 ± 15	14.6 ± 1.5
		Muri11B-80-2	8.89 ± 0.29	51 ± 9	61 ± 16	25.3 ± 2.8
		Muri11B-97-1	6.31 ± 0.09	42 ± 9	41 ± 16	40.2 ± 1.9
		Muri11B-428-1	4.30 ± 0.07	28 ± 10	74 ± 15	183.6 ± 8.1
Y	Indarch	Feb-25-10-10	102.8 ± 1.0	−17 ± 5	17 ± 6	8.6 ± 0.8
		Feb-25-19-7	112.2 ± 1.6	−12 ± 7	11 ± 8	11.1 ± 1.5
		Feb-25-22-4	101.3 ± 1.7	−11 ± 7	3 ± 7	6.0 ± 0.8
		Feb-25-6-2	123.2 ± 1.3	125 ± 5	126 ± 6	6.6 ± 1.5
		Feb-25-9-13	102.9 ± 1.1	−3 ± 6	23 ± 6	7.1 ± 1.2
		Oct-16-3-7	142.6 ± 3.4	−9 ± 9	32 ± 12	4.6 ± 0.8
		Oct-16-4-6	118.2 ± 1.8	−67 ± 7	39 ± 9	10.6 ± 7.5
		Oct-17-10-11	361.4 ± 17.6	85 ± 6	193 ± 8	22.6 ± 0.8
		Oct-17-10-5	107.6 ± 1.6	3 ± 6	21 ± 8	7.8 ± 1.0
		Oct-17-16-21	170.8 ± 4.5	−12 ± 7	39 ± 10	4.5 ± 1.1
		Oct-17-3-15	104.5 ± 1.5	31 ± 5	52 ± 8	5.9 ± 0.2
		Oct-17-8-3	105.9 ± 1.7	−37 ± 7	−17 ± 9	4.5 ± 0.7
		IH6-12-2	116.3 ± 0.9	3 ± 5	52 ± 7	8.5 ± 0.6
		IH6-13-5	134.8 ± 1.2	−13 ± 5	16 ± 7	43.8 ± 2.7
		IH6-16-2	149.1 ± 1.4	−38.2 ± 5.6	38.7 ± 7.3	4.7 ± 1.8
X	Indarch	Oct-16-10-18	275.0 ± 9.6	−407 ± 7	−525 ± 9	379 ± 25
		Oct-17-2-4	53.9 ± 0.5	−462 ± 6	−471 ± 8	2185 ± 22
Z	Indarch	Feb-25-10-11	71.6 ± 0.5	−117 ± 5	132 ± 5	8.1 ± 1.2
		Feb-25-10-9	54.7 ± 0.3	−116 ± 5	99 ± 6	1.3 ± 0.1
		Feb-25-20-12	98.0 ± 0.9	−8 ± 5	40 ± 6	7.3 ± 2.1
		Feb-25-6-4	74.9 ± 0.7	−32 ± 6	19 ± 7	10.5 ± 3.2
		Feb-25-7-11	42.6 ± 0.2	−65 ± 5	49 ± 5	11.6 ± 1.0
		Feb-25-9-5	57.9 ± 0.4	−12 ± 5	32 ± 5	10.3 ± 1.4
		Oct-16-2-1	78.1 ± 0.8	−37 ± 6	25 ± 8	17.8 ± 3.3
		Oct-16-3-24	75.7 ± 0.9	−23 ± 7	33 ± 10	9.2 ± 1.6
		Oct-17-10-10	50.4 ± 0.4	−26 ± 5	50 ± 8	11.2 ± 0.8
		Oct-17-10-21	59.4 ± 0.5	−64 ± 6	63 ± 9	6.1 ± 1.7
		Oct-17-2-8	57.0 ± 0.6	−106 ± 7	12 ± 10	6.0 ± 1.1
		Oct-17-4-7	96.5 ± 1.4	−16 ± 6	37 ± 8	8.0 ± 1.4
		IH6-4-6	48.4 ± 0.4	−124 ± 5	140 ± 8	4.7 ± 0.3
		IH6-8-1	57.9 ± 0.4	−23 ± 5	28 ± 7	7.3 ± 0.5
		IH6-11-11	40.2 ± 0.4	−81 ± 7	1 ± 9	8.3 ± 1.1
		IH6-12-1	50.3 ± 0.3	−35 ± 5	30 ± 7	8.0 ± 0.6
		IH6-16-1	51.0 ± 0.4	−59 ± 6	23 ± 8	6.7 ± 1.3
	Murchison	Mur-13-1	41.3 ± 1.6	−141 ± 25	29 ± 28	7.2 ± 1.0
		Mur-13-3	54.0 ± 1.8	−81 ± 18	36 ± 20	9.0 ± 1.8

Table 3 (*continued*)

Type	Meteorite	Grain	$^{12}C/^{13}C \pm 1\sigma$	$\delta^{29}Si/^{28}Si \pm 1\sigma$ (‰)	$\delta^{30}Si/^{28}Si \pm 1\sigma$ (‰)	$^{26}Al/^{27}Al \pm 1\sigma$ ($\times 10^4$
Mainstream	Indarch	IH6-3-7	47.5 ± 0.5	64 ± 7	64 ± 9	3.0 ± 1.0
		IH6-3-9	55.1 ± 0.6	47 ± 7	42 ± 9	8.3 ± 0.7
		IH6-4-2	45.3 ± 0.4	101 ± 6	95 ± 8	4.2 ± 0.6
		IH6-4-3	60.2 ± 0.5	-7 ± 5	15 ± 7	7.4 ± 1.0
		IH6-4-7	40.4 ± 0.3	6 ± 5	24 ± 7	3.8 ± 0.5
		IH6-5-11	95.9 ± 1.0	18 ± 6	49 ± 8	18.2 ± 6.9
		IH6-5-12	39.7 ± 0.3	48 ± 6	63 ± 8	3.2 ± 1.1
		IH6-6-1	10.7 ± 0.1	-21 ± 6	17 ± 8	4.8 ± 1.6
		IH6-8-3	62.8 ± 0.5	64 ± 6	64 ± 8	7.6 ± 1.2
		IH6-8-5	85.6 ± 0.7	7 ± 5	30 ± 7	5.3 ± 0.4
		IH6-11-2	53.7 ± 0.4	78 ± 5	83 ± 7	8.3 ± 1.1
		IH6-11-7	42.4 ± 0.3	80 ± 6	69 ± 8	14.8 ± 0.5
		IH6-11-10	74.9 ± 0.6	31 ± 5	60 ± 7	4.6 ± 0.9
		IH6-11-14	54.6 ± 0.4	50 ± 6	46 ± 8	5.4 ± 0.5
		IH6-12-4	69.7 ± 0.5	7 ± 6	36 ± 7	3.9 ± 1.3
		IH6-12-10	59.3 ± 0.5	31 ± 6	53 ± 8	10.7 ± 0.8
		IH6-13-2	73.7 ± 0.7	11 ± 6	22 ± 8	3.8 ± 0.4
		IH6-16-7	48.7 ± 0.3	-12 ± 5	8 ± 7	4.3 ± 1.5

considerably. Inferred $^{26}Al/^{27}Al$ ratios are plotted against $^{12}C/^{13}C$ ratios in Fig. 5 and the two previously reported Z grain data are included in the table. Also plotted in the figure are theoretical predictions for the composition of the envelope of AGB stars of different mass and metallicity during third dredge-up (TDU) after consecutive thermal

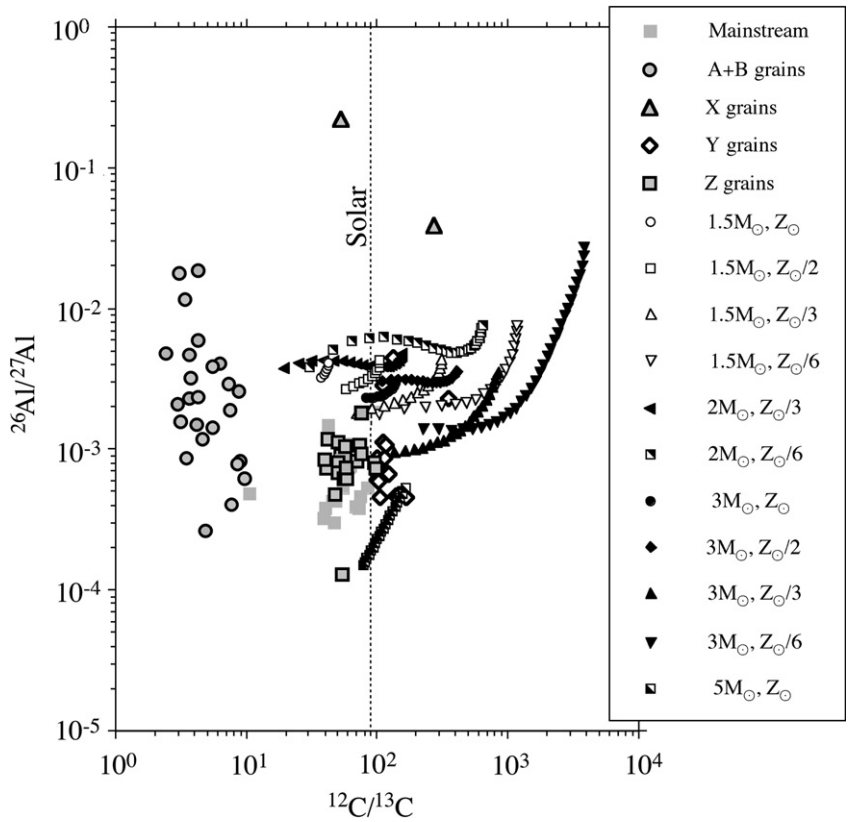

Fig. 5. Aluminum isotopic ratios, inferred from ^{26}Mg excesses, of SiC grains from Indarch IH6 are plotted against their C isotopic ratios. Also plotted are theoretical predictions for the $^{26}Al/^{27}Al$ and $^{12}C/^{13}C$ ratios in the envelope of AGB stars of different masses and metallicities for consecutive TDUs following thermal pulses in these stars. Predicted ratios are plotted only for $C > O$ in the envelope, a necessary condition for the condensation of SiC grains. Predictions are for different stellar masses and metallicities. The Reimers mass loss parameter η is assumed to be 0.3 for the 1.5 $M_\odot$ models, 0.5 for the 2 $M_\odot$ models, 1.5 for the 3 $M_\odot$ models, and 10 for the 5 $M_\odot$ models.

pulses. Plotted are only compositions after the envelope became C-rich (C > O), i.e., after the star turned into a carbon star, necessary for the condensation of SiC.

As already mentioned, in low-mass AGB stars, ^{26}Al is produced in the H-burning shell by proton capture on ^{25}Mg and mixed into the envelope by the TDU. In intermediate-mass stars, hot bottom burning, when the convective envelope reaches into the H-burning shell, can give rise to high ^{26}Al abundances in the envelope (Lattanzio et al., 1997; Mowlavi and Meynet, 2000; Karakas and Lattanzio, 2003). However, hot bottom burning generally prevents carbon-star formation (Frost and Lattanzio, 1996; Zinner et al., 2006b).

The models plotted in Fig. 5 do not include cool bottom processing (CBP) (Wasserburg et al., 1995, 2006; Nollett et al., 2003). In this process material is slowly circulating from the bottom of the convective envelope to hot regions close to the H-burning shell. It originally has been proposed to occur in low-mass stars on the red giant branch (RGB) and has been invoked in order to explain low ^{12}C/^{13}C ratios in RGB stars and low ^{18}O/^{16}O ratios in many presolar oxide grains (Charbonnel, 1995; Wasserburg et al., 1995; Abia and Isern, 1997; Boothroyd and Sackmann, 1999). Nollett et al. (2003) applied CBP also to TP-AGB stars to explain the high ^{26}Al/^{27}Al ratios observed in many presolar oxide grains (see also Wasserburg et al., 2006). Fig. 6 shows a comparison of ^{26}Al/^{27}Al ratios in presolar oxide and presolar SiC grains. It is clear that ratios in oxide grains are much higher than those of SiC grains believed to have an AGB origin (mainstream, Y, and Z grains). Figs. 5 and 6 also show that, with the exception of a few mainstream grains, the ^{26}Al/^{27}Al ratios of mainstream, Y, and Z grains are within the range predicted by AGB models without any CBP.

This is not unexpected for mainstream and Y grains, but is puzzling for Z grains. The reason is that while the Si isotopic ratios of Z grains can be explained by assuming that they come from low-metallicity AGB stars (Hoppe et al., 1997), the C isotopic ratios predicted for such stars are much higher than those observed. This can be seen in Fig. 5 where the predicted ^{12}C/^{13}C ratios in the envelope of low-metallicity AGB stars reach values in excess of 1000, whereas essentially all Z grains have ratios smaller than 100. As it has been for the low ^{12}C/^{13}C ratios in RGB stars (Charbonnel, 1995; Abia and Isern, 1997; Boothroyd and Sackmann, 1999), CBP during the AGB phase has been invoked to explain the low ^{12}C/^{13}C ratios in Z grains (Hoppe et al., 1997; Nittler and Alexander, 2003; Nittler et al., 2005b; Zinner et al., 2006b). For oxide grains (Fig. 6) CBP on the AGB can explain low ^{18}O/^{16}O ratios (Wasserburg et al., 1995; Boothroyd and Sackmann, 1999) and high ^{26}Al/^{27}Al ratios (Nollett et al., 2003). For Z grains CBP apparently can lower ^{12}C/^{13}C ratios but does not result in higher ^{26}Al/^{27}Al ratios and this is startling. However, it is not impossible. The basic physical mechanism that drives CBP is still not understood. In their parametric model Nollett et al. (2003) assume two parameters to characterize CBP: the rate of circulation of material into hot zones and the maximum temperature reached by that material. In their effect on the ^{12}C/^{13}C and^{18}O/^{16}O ratios, and the ^{26}Al/^{27}Al ratios in the envelope these two parameters are almost independent. The first two ratios are mostly affected by the circulation rate and the third mostly by the temperature reached by the circulating matter (see Fig. 6 in Nollett et al., 2003). The reason is that the ^{18}O(p,α)^{15}N reaction, which destroys ^{18}O, can take place at a much lower temperature than the ^{25}Mg(p,γ)^{26}Al reaction. The general trend of high ^{26}Al/^{27}Al ratios being associated with low ^{18}O/^{16}O ratios in Fig. 6 indicates that the two parameters in the CBP model are not completely independent. On the other hand, the large scatter in the data points must

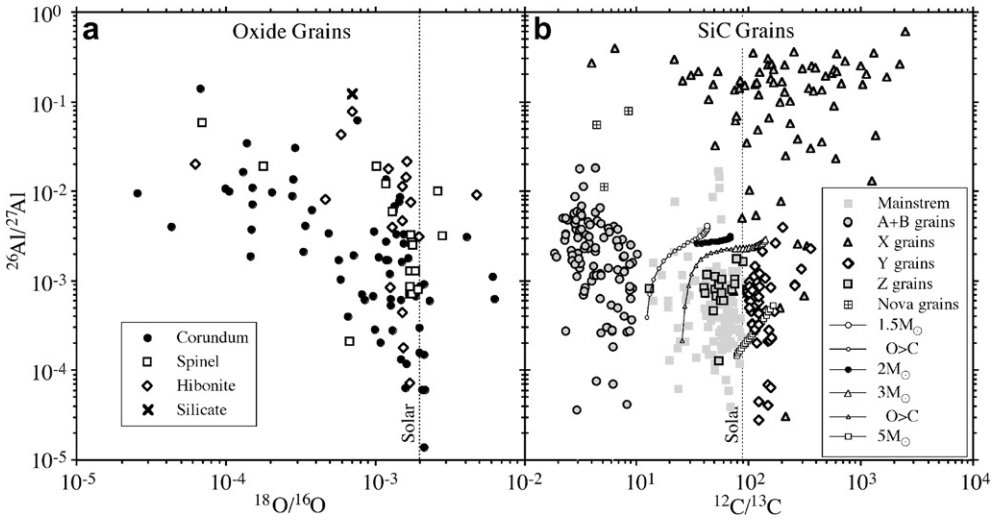

Fig. 6. Inferred ^{26}A1/^{27}A1 ratios are plotted against ^{18}O/^{16}O ratios in presolar oxide grains and one silicate grain (a) and against ^{12}C/^{13}C ratios in presolar SiC grains (b) are theoretical predictions for AGB stars of solar metallicity. For the 1.5 and 3 M$_\odot$ models the evolution of the Al and C isotopic ratios is shown for O-rich (O > C, small symbols) and C-rich (C > O, large symbols) stars, for the 2 and 5 M$_\odot$ models prediction for only C-rich stars are shown. The oxide grain data are from Nittler et al. (1997, 2005a), Choi et al. (1998, 1999), Nguyen and Zinner (2004) and Zinner et al. (2006b,a), the SiC grain data are from Alexander (1993), Hoppe et al. (1994, 1996b), Nittler et al. (1995), Huss et al. (1997), Amari et al. (2001a,b,c), Nittler and Hoppe (2005), and this study.

mean that either the one or the other parameter can dominate in a given star. The $^{12}C(p,\gamma)^{13}N$ reaction (^{13}N decays to ^{13}C) is also activated at much lower temperatures than the $^{25}Mg(p,\gamma)^{26}Al$ reaction. Thus it is possible that in the parent stars of Z grains the circulation rate was high but the material never experienced high enough temperatures for significant ^{26}Al production.

There exists one important difference between presolar oxide and SiC grains: the former come from stars with O > C, the latter from stars with O < C. The Nollett et al. (2003) model suggests that for high circulation rates CBP prevents AGB stars from becoming carbon stars. The new solar abundances result in higher C/O ratios but even then the destruction of ^{12}C during CBP could result in C/O < 1. We want to emphasize that the circulation rate and maximum temperature in CBP are still treated in a parametric way and are not constrained by any well-understood physical mechanisms. Zinner et al. (2005b) considered a different mix of these two parameters to explain the difference in the $^{26}Al/^{27}Al$ ratios between oxide and SiC grains. Both oxide grains with low $^{18}O/^{16}O$ and high $^{26}Al/^{27}Al$ ratios, and Z type SiC grains must have come from AGB stars that experienced CBP but this process might have proceeded in different ways in O- and C-rich stars: in the former the circulated material reached higher temperatures than in the latter. Another possible difference between oxide and Z grains is that they originated from stars with different metallicities. The Si isotopic ratios of Z grains indicate low-metallicity parent stars. Nittler and coworkers (Nittler et al., 1997; Alexander and Nittler, 1999; Nittler, 2005) have estimated the metallicities of the parent stars of group 1 and 3 oxide grains from the inferred original O isotopic compositions of their parent stars before they were modified by first and second dredge-up (Boothroyd et al., 1994; Boothroyd and Sackmann, 1999). However, this procedure can be applied only to grains whose parent stars did not experience CBP, which lowered their $^{18}O/^{16}O$ ratios, and not to group two grains with low $^{18}O/^{16}O$ and high $^{26}Al/^{27}Al$ ratios. Another possibility that has previously been considered (Zinner et al., 2005b) is that presolar oxide and SiC grains come from stars with different mass. According to the FRANEC stellar code, stars of solar metallicity with 1.5 $M_\odot$ and a high mass loss never become C-rich because the number of TDU is small and not enough ^{12}C is dredged up into the envelope (see Table 1 of Zinner et al., 2006b). However, the observed $^{17}O/^{16}O$ ratios of group 2 oxide grains suggest that these mostly formed in stars less massive than 1.5 $M_\odot$.

Unfortunately, at present we do not understand the physical mechanism of CBP well enough to be able to say why this process proceeds differently in the parent stars of oxide grains than in the low-metallicity parent stars of Z grains, and what stellar parameters such as mass, metallicity, mass loss, and rotation rate are responsible for these differences.

4.3. Titanium isotopic ratios of presolar SiC grains of type Z

4.3.1. Grain data

We measured the Ti isotopic ratios of three A + B grains, two Y grains, five Z grains from Indarch, and four mainstream grains, one Y grain and four Z grains from Murchison (Table 4). The C and Si isotopic ratios of the Indarch grains were measured in this study. Those of the Murchison grains had previously been determined at the Carnegie Institution during automatic imaging searches. The Murchison data have been mentioned by Nittler and Hoppe (2005), but have not been reported in detail. Fig. 7 shows the Si isotopic ratios of these Z grains, which include two Z grains whose Si and Ti isotopic ratios had previously been reported (Amari et al., 2005). Also shown in the figure for comparison are the Si isotopic ratios of other Z, mainstream and X grains. The Ti and Si isotopic patterns (plotted as δ-values) of Z grains and of mainstream grains whose Ti and Si isotopic ratios had been measured previously (Hoppe et al., 1994; Alexander and Nittler, 1999) are shown in Fig. 8-1 and 8-2. The reference isotopes ^{28}Si and ^{48}Ti are α nuclei, whose evolution in the Galaxy is believed to be different from that of the other Si and Ti isotopes. The α nuclei are preferentially produced in early supernovae. It can be seen that the isotopic patterns differ between the Z and mainstream grains, especially if we compare the average patterns indicated by large open circles. In the mainstream grains all Si and Ti isotopes are enhanced relative to ^{28}Si and ^{48}Ti whereas in Z grains only ^{30}Si and ^{50}Ti are enhanced while the other isotopes are depleted. Thus the Ti isotopes $^{46,47,49}Ti$ resemble ^{29}Si, while ^{50}Ti resembles ^{30}Si. The behavior of the former group is apparently mostly determined by Galactic chemical evolution (GCE), while the latter pair is mostly influenced by neutron-capture nucleosynthesis in the parent AGB stars.

The correlations between different Ti isotopic ratios and between Ti and Si isotopic ratios is best seen on plots where isotopic ratios are plotted against one another. In Fig. 9-1 and 9-2 we present Ti 3-isotope δ-value plots of the 11 Z grains together with mainstream, A + B, and Y grains (Hoppe et al., 1994; Alexander and Nittler, 1999; Amari et al., 2001b,c). In both figures we compare the data with AGB models using two different strengths of the ^{13}C pocket (ST and ST/6). As can be seen in the figure, the compositions of the Z grains extend the correlations previously obtained for the mainstream grains (the solid lines in the plots) to lower Ti isotopic ratios. An exception is the $\delta^{50}Ti/^{48}Ti$ vs $\delta^{46}Ti/^{48}Ti$ plot where the Z grains plot above the mainstream correlation line. This situation is similar to that of the Si isotopic ratios where Z grains plot to the right of the mainstream correlation line (see Fig. 7). The Ti isotopic ratios confirm the interpretation based on the Si isotopic ratios that Z grains come from low-metallicity parent stars. As do the Si isotopic ratios, the Ti isotopic ratios relative to ^{48}Ti increase with increasing metallicity during GCE. Fig. 10 shows that the general correlation between $^{46,47,49}Ti/^{48}Ti$ ratios and the $^{29}Si/^{28}Si$ ratio previously observed for mainstream grains also holds for Z grains.

4.3.2. Comparison with AGB models

Mainstream grains are believed to mainly originate from AGB stars of near solar metallicity. For such stars the predicted isotopic shifts in Si and Ti are small and the correlation lines for mainstream grains are thus considered to

Table 4
Si and Ti isotopic compositions

Grain	Type	$\delta^{29}Si/^{28}Si \pm 1\sigma$ (‰)	$\delta^{30}Si/^{28}Si \pm 1\sigma$ (‰)	$\delta^{46}Ti/^{48}Ti \pm 1\sigma$ (‰)	$\delta^{47}Ti/^{48}Ti \pm 1\sigma$ (‰)	$\delta^{49}Ti/^{48}Ti \pm 1\sigma$ (‰)	$\delta^{50}Ti/^{48}Ti \pm 1\sigma$ (‰)	$\Delta^{30}Si/^{28}Si \pm 1\sigma$ (‰)	$\Delta^{50}Ti/^{48}Ti \pm 1\sigma$ (‰)[a]
Indarch									
Oct-17-10-23	A + B	41 ± 5	110 ± 8	−65 ± 35	9 ± 38	−18 ± 43	408 ± 54		
Oct-17-15-1	A + B	43 ± 5	43 ± 8	−56 ± 42	26 ± 47	93 ± 56	−45 ± 53		
Oct-17-8-18	A + B	42 ± 6	32 ± 8	−25 ± 32	−104 ± 32	−29 ± 38	−124 ± 37		
Feb-25-18-5	Y	−40 ± 15	−10 ± 19	−122 ± 45	−113 ± 50	−33 ± 60	200 ± 71	9 ± 23	466 ± 146
Oct-17-3-15	Y	31 ± 5	52 ± 8	−47 ± 31	−46 ± 32	35 ± 39	132 ± 41	21 ± 9	213 ± 99
Feb-25-10-11	Z	−117 ± 5	132 ± 5	−188 ± 51	−168 ± 57	−168 ± 66	151 ± 83	232 ± 7	560 ± 174
Feb-25-20-12	Z	−8 ± 5	40 ± 6	−53 ± 35	−90 ± 38	−34 ± 45	373 ± 58	40 ± 7	512 ± 116
Oct-16-2-1	Z	−37 ± 6	25 ± 8	−122 ± 21	−98 ± 21	−57 ± 25	94 ± 27	47 ± 10	341 ± 91
Oct-17-10-10	Z	−26 ± 5	50 ± 8	−177 ± 29	−126 ± 31	−117 ± 36	82 ± 42	65 ± 9	453 ± 120
Oct-17-3-24	Z	−17 ± 6	33 ± 8	−138 ± 63	−79 ± 71	47 ± 87	−31 ± 87	38 ± 10	230 ± 185
Murchison									
Muri11B-179-1	M	182 ± 8	158 ± 15	184 ± 17	76 ± 17	236 ± 19	334 ± 34		
Muri11B-236-1	M	136 ± 9	123 ± 14	169 ± 10	63 ± 15	139 ± 9	229 ± 13		
Muri11B-475-1	M	105 ± 8	96 ± 15	42 ± 7	13 ± 11	129 ± 5	231 ± 15		
Muri11B-34-9	Y	18 ± 11	60 ± 19	25 ± 50	53 ± 52	130 ± 60	386 ± 77	41 ± 22	349 ± 148
249_1[b]	Z	−130 ± 5	201 ± 6	−280 ± 20	−145 ± 20	−184 ± 20	−66 ± 25	321 ± 8	515 ± 135
415_3[b]	Z	−108 ± 5	392 ± 6	−341 ± 16	−185 ± 16	−209 ± 14	276 ± 26	519 ± 9	1060 ± 165
Muri11B-123-4	Z	−60 ± 10	63 ± 17	−52 ± 55	−42 ± 59	−232 ± 59	29 ± 75	109 ± 19	103 ± 157
Muri11B-135-1	Z	−155 ± 10	107 ± 17	−298 ± 31	−171 ± 35	−282 ± 37	4 ± 46	235 ± 19	639 ± 158
Muri11B-476-6	Z	7 ± 11	223 ± 20	−240 ± 36	−81 ± 68	−117 ± 42	223 ± 59	234 ± 22	765 ± 156
Muri11B-204-1	Z	−91 ± 16	48 ± 21	−207 ± 31	−162 ± 32	−166 ± 32	92 ± 51	116 ± 25	534 ± 134

[a] The $\Delta^{30}Si/^{28}Si$ (‰) and $\Delta^{50}Ti/^{48}Ti$ (‰) values express the shifts in these isotopic ratios due to AGB nucleosynthesis. See text.
[b] Data on these two Z grains from Murchison have previously been reported by Amari et al. (2005).

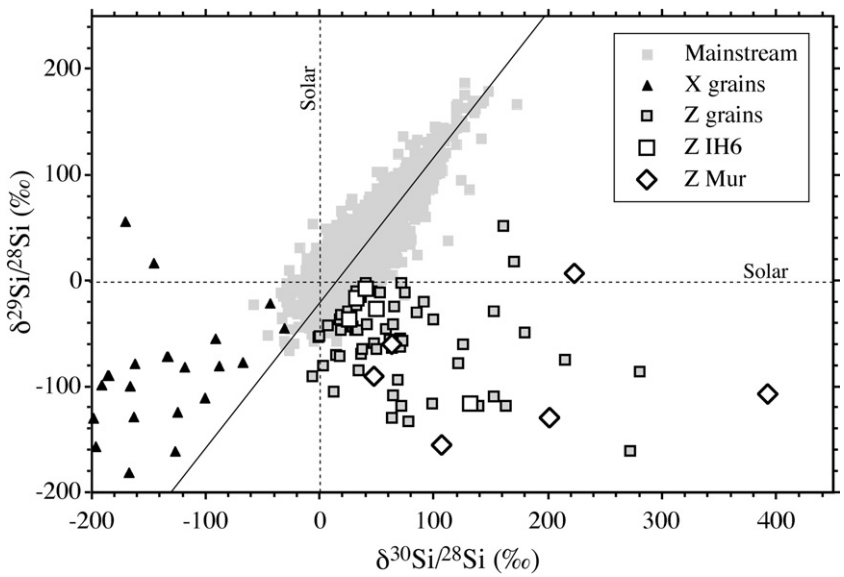

Fig. 7. Silicon isotopic ratios of the Z grains whose Ti isotopic ratios were measured (Table 4) are shown as large open symbols. The Si isotopic ratios of mainstream, X, and other Z grains are shown for comparison. Here and in Figs. 9 and 10 the broken black lines indicate the solar isotopic ratios. The solid line is the mainstream correlation line (see Appendix). The reason for some overlap between mainstream and Z grains is that overlapping mainstream grains have large errors. Data are from Alexander (1993), Hoppe et al. (1994, 1996b), Nittler et al. (1995), Huss et al. (1997), Lin et al. (2002), Nittler and Alexander (2003), Amari et al. (2005), and this study.

mostly reflect Galactic evolution effects. This assumption is strengthened by the fact that the mainstream correlation lines in Figs. 9 and 10 pass close to the origin (i.e., the solar isotopic compositions). In the upper two panels of Fig. 9-1 and 9-2 the data points for the Z grains plot close to the mainstream correlation lines. This must either mean that even in low-metallicity stars the ^{46,47,49}Ti/^{48}Ti ratios are not affected very much by AGB nucleosynthesis or that the individual isotopic shifts due to neutron capture are such that in 3-isotope plots such as in Fig. 9-1 and 9-2 the resulting theoretical shifts are parallel to the trend due to GCE. This might indeed be the case. In Fig. 9-1 and 9-2 we also plot the Ti isotopic compositions theoretically predicted for the envelope of TP-AGB stars during repeated TDU for 1.5, 2, and 3 $M_\odot$ stars with 1/3 and 1/6 solar metallicity. These models assumed a Reimers parameter $\eta = 0.3$ for 1.5 $M_\odot$, $\eta = 0.5$ for 2 $M_\odot$, and $\eta = 1.5$ for 3 $M_\odot$ as well as initial δ^iTi/^{48}Ti values of −260‰ and −378‰ for the metallicities $Z = 0.006$ ($Z_\odot/3$) and $Z = 0.003$ ($Z_\odot/6$), respectively, as explained in Section 4.1. In Fig. 9-1 we assumed the ST ^{13}C pocket, in Fig. 9-2 we assumed a ^{13}C pocket of ST/6 (d6). Final Ti and Si isotopic ratios are given in Table 5 also for ST/3 (d3) and ST/12 (d12) pockets. As can be seen from Fig. 9-1 and 9-2 and from Table 5, the final ^{50}Ti/^{48}Ti ratios predicted for the envelope depend on the strength of the ^{13}C pocket. This is in contrast to the Si isotopes, which are only minimally affected by the ^{13}C neutrons (see Fig. 7 of Zinner et al., 2006b).

In panel (a) of Fig. 9-1 and 9-2 (δ^{47}Ti/^{48}Ti vs. δ^{46}Ti/^{48}Ti plots) the predicted isotopic evolution occurs almost exactly parallel to the mainstream (+Z grain) correlation line but our assumed initial compositions of the parent stars completely miss the grain data. We assumed that the abundance of all the Ti isotopes except ^{48}Ti evolved in the same way as a function of increasing metallicity, resulting in slope-one lines in 3-isotopes plots such as those in Fig. 9-1 and 9-2. In these figures we also plotted lines of the evolution of the Ti isotopes as function of metallicity (broken gray lines) predicted by normalized GCE models (Timmes et al., 1995; see Fig. 5 of Alexander and Nittler, 1999). As has been done by Alexander and Nittler (1999), we normalized the Timmes et al. (1995) predictions by forcing the Ti isotopic ratio to agree with the solar ratios at solar metallicity. In the δ^{47}Ti/^{48}Ti vs δ^{46}Ti/^{48}Ti and δ^{50}Ti/^{48}Ti vs δ^{46}Ti/^{48}Ti plots this line is close to our assumed initial ratios (the large open symbols) for low-metallicity stars but differs in the δ^{49}Ti/^{48}Ti vs δ^{46}Ti/^{48}Ti plot. However, it has to be said that while the Timmes et al. (1995) lines closely approach our assumed initial ratios in panels (a) and (c), the actual δ-values corresponding to a given metallicity are quite different. In the Timmes et al. GCE model the Ti isotopic ratios decrease much more rapidly with decreasing metallicity than we assumed. For example for $Z = 0.006$ the δ^{47}Ti/^{48}Ti value by Timmes et al. is −776‰ (if we normalized the ratios to solar at solar metallicity), whereas our assumed value is −378‰.

We should point out that the mainstream correlation lines represent the GCE of the Ti isotopes only approximately because the Ti isotopic ratios of mainstream grains are also affected by AGB nucleosynthesis. Alexander and Nittler (1999) and Amari et al. (2001b) have subtracted this contribution in order to obtain the GCE lines. If we did that under the assumption, made by these authors, that all mainstream grains originated from stars of solar metallicity and that the shifts are calculated with the ST ^{13}C pocket, the mainstream correlation lines would be shifted up by between 10‰ and 15‰ for the top panel, shifted down by between 45‰ and 112‰ for the middle panel,

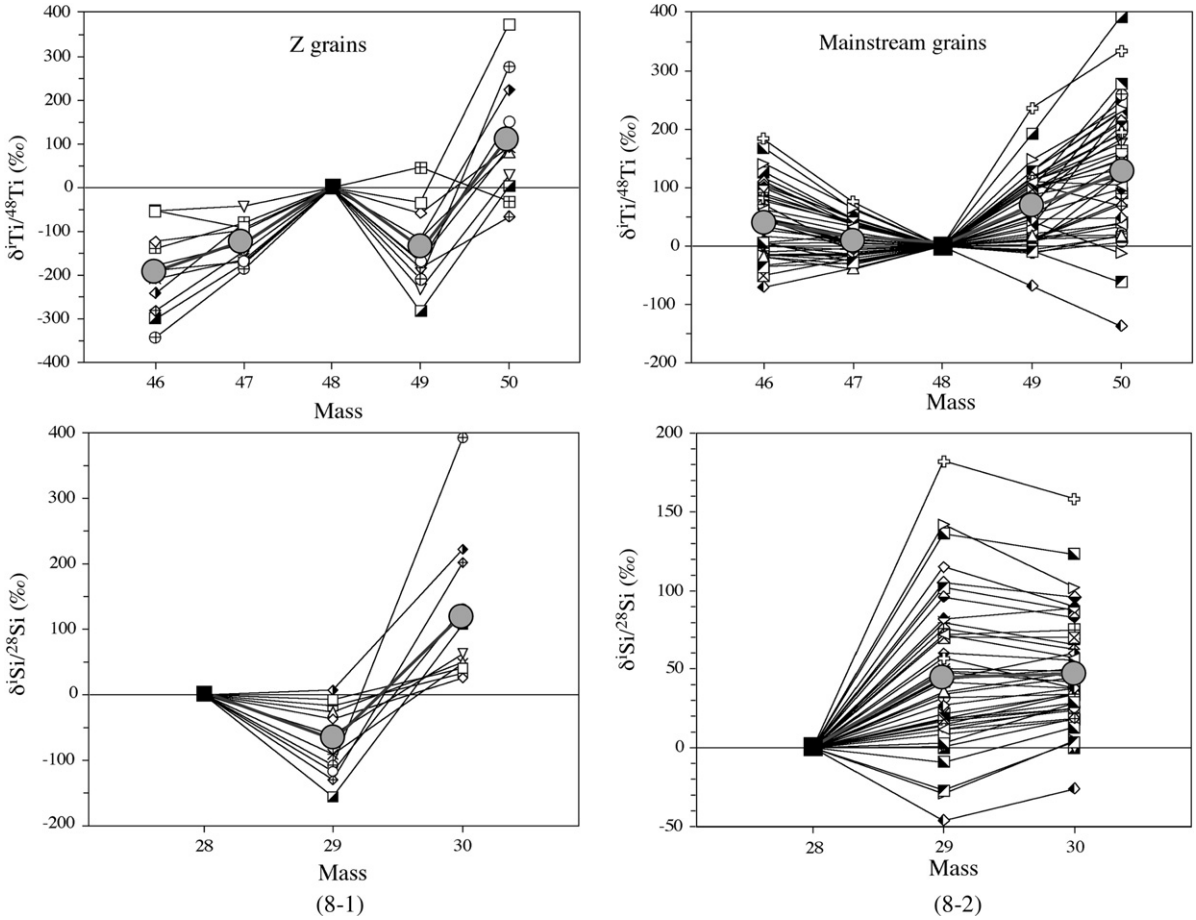

Fig. 8. Titanium and Si isotopic patterns of Z grains (8-1) and mainstream grains (8-2). Isotopic ratios of individual grains are plotted as δ-values relative to the reference isotopes ^{48}Ti and ^{28}Si. The large gray circles indicate average Ti and Si ratios. In both figures the same symbols are used for the Si and Ti isotopic ratios of individual grains. The mainstream data are from Hoppe et al. (1994) and Alexander and Nittler (1999).

and down by between 79‰ and 186‰ for the bottom panel, depending on stellar mass (Table 5). There are several reasons that we do not show these lines in Fig. 9-1 and 9-2. First, the shifts depend on stellar mass, which is not known a priori. Second, the assumption that all mainstream grains originated from stars of solar metallicity is an oversimplification. These grains probably came from stars with a range of metallicity and, correspondingly, the nucleosynthetic shifts would cover a certain range. One could certainly model this dependence by interpolating between theoretical predictions of isotopic shifts for different metallicities. We might do so in the future. At present, there are large uncertainties in such an endeavor because, third, as can already be seen in Fig. 9-1 and 9-2 and will be discussed below, the theoretical predictions for the ^{49}Ti/^{48}Ti and ^{50}Ti/^{48}Ti ratios in low-metallicity stars (panels (b) and (c)) do not match the grain data very well. We therefore do not know whether theoretical predictions for Ti isotopic shifts in AGB stars with metallicities close to that of the Sun would be very realistic.

As already mentioned, in the δ^{47}Ti/^{48}Ti vs δ^{46}Ti/^{48}Ti plot, the predicted isotopic compositions completely miss the grain data. This is a strong indication that our assumed initial isotopic compositions and those obtained from the Timmes et al. (1995) GCE model are not correct and that these two isotopic ratios evolve along a line with a slope of approximately one half. The production of the Ti isotopes, especially that of ^{47}Ti, is not well understood. In the GCE model of Timmes et al. (1995) the predicted ^{48}Ti abundance is a factor of two lower than solar and the ^{47}Ti/^{48}Ti ratio is almost a factor of three smaller than the solar ratio at solar metallicity. For the Timmes et al. (1995) GCE lines shown in Fig. 9-1 and 9-2 we followed Alexander and Nittler (1999) and normalized all Ti isotopic ratios to solar for stars of solar metallicity.

We can gain some additional insight into the GCE of Ti isotopes at lower-than-solar metallicity by considering the composition of a presolar Al_2O_3 grain, S-C261, reported by Choi et al. (1998). This grain showed large depletions of ^{46,47,49,50}Ti relative to ^{48}Ti and the solar composition. A comparison of the O isotopic composition of this grain with the first dredge-up calculations of Boothroyd and Sackmann (1999) suggests that it formed in a star of $\sim 2\ M_\odot$ and $\sim 65\%\ Z_\odot$ ($Z = 0.013$). Moreover, its inferred ^{26}Al/^{27}Al ratio of $\sim 6 \times 10^{-4}$ indicates that it formed fairly early on the AGB (cf. Fig. 6). Its Ti isotopic composition

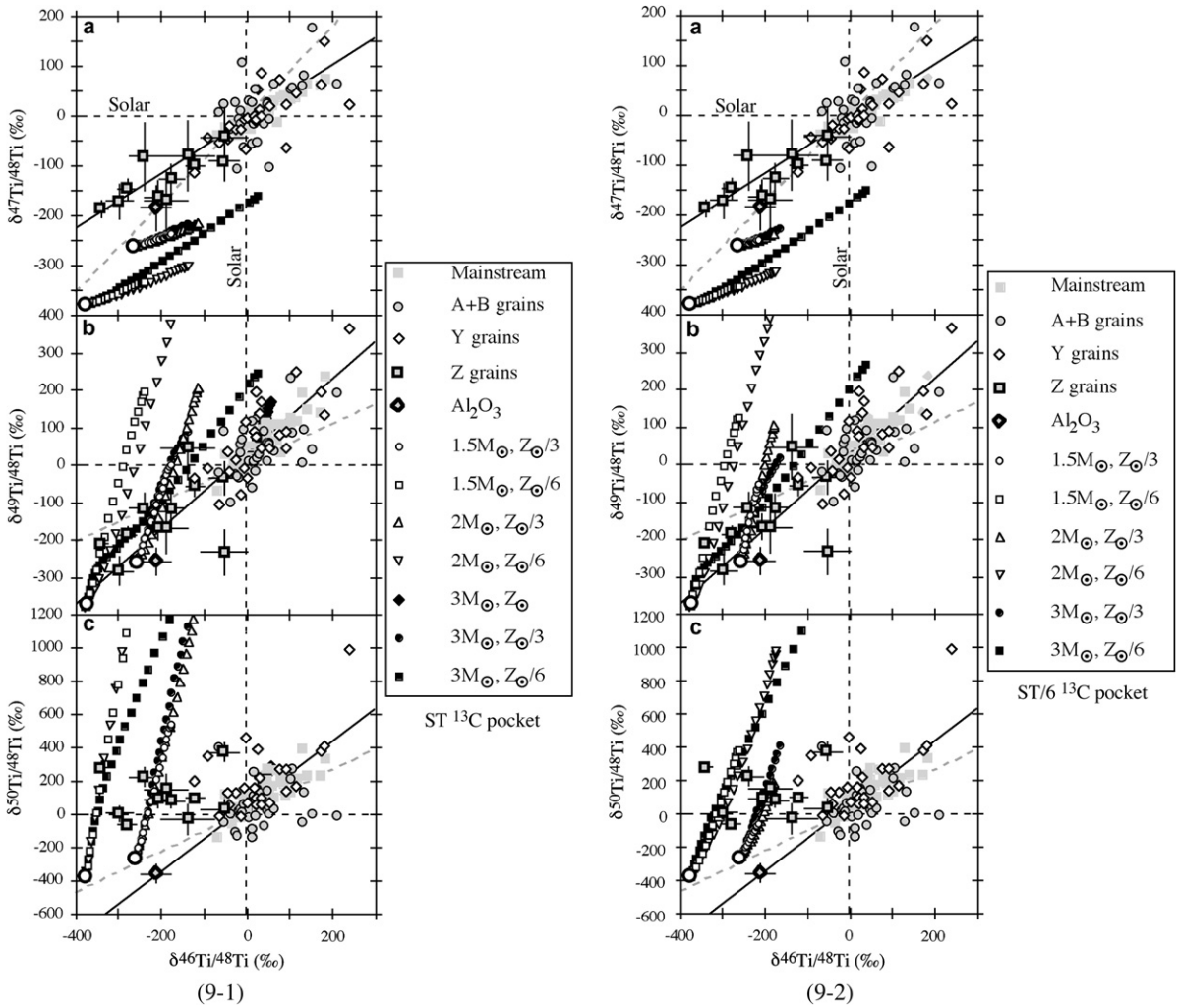

Fig. 9. Titanium isotopic ratios of presolar SiC grains and one presolar Al_2O_3 grain are plotted as δ-values in 3-isotope plots. The solid lines are least-square fits to the Ti isotopic ratios of mainstream grains. The gray broken lines indicate the normalized GCE evolution of the Ti isotopic ratios calculated by Timmes et al. (1995); see also Alexander and Nittler (1999). Also plotted are theoretical predictions for the envelope compositions of C-rich AGB stars during repeated TDU episodes for 1.5, 2, and 3 $M_\odot$ models with solar (for the 3 $M_\odot$ model), 1/3, and 1/6 solar metallicity for the standard (ST) ^{13}C pocket (9-1) and for 1/6 of the standard pocket (9-2). The large open circles depict the assumed initial compositions of low-metallicity stars. Data for mainstream, A + B, and Y grains are from this study, Hoppe et al. (1994), Alexander and Nittler (1999), and Amari et al. (2001b,c), data for the Al_2O_3 grain from Choi et al. (1998).

should thus have been affected by neutron capture to a much lesser degree than that of the SiC parent stars and its composition should be a good indication of the true GCE Ti isotopic trends. As indicated on Fig. 9, the composition of this grain lies very close to the extensions of the mainstream correlation lines, supporting the inference that the $\delta^{47}Ti/^{48}Ti$ vs $\delta^{46}Ti/^{48}Ti$ slope is shallower than assumed by us for the initial AGB compositions and given by the normalized Timmes et al. model.

In the $\delta^{49}Ti/^{48}Ti$ vs $\delta^{46}Ti/^{48}Ti$ plots (graphs (b) in Fig. 9-1 and 9-2) the Z grain data points also plot close to the mainstream correlation line. However, in this case, with the exception of the 3 $M_\odot$ $Z = 0.003$ model, the evolution of the Ti isotopes during repeated TDUs points away from the mainstream line. The predicted shifts for the 1.5 $M_\odot$ and 3 $M_\odot$ $Z = 0.006$ models (possibly also for 2 $M_\odot$ and ST/6) are small enough to be roughly compatible with the grain data, however they range far above the grain data for the 1.5 and 2 $M_\odot$ $Z = 0.003$ models, for the ST as well as ST/6, and even ST/12 pockets (see Table 5). The trajectory of the Ti isotopic evolution for the 3 $M_\odot$ $Z = 0.003$ models is quite different from those of the lower-mass models. It snakes along the mainstream line and there is essentially no effect of the strength of the ^{13}C pocket. One Z grain, Muri11B-123-4 (see Table 4), with a moderate ^{46}Ti depletion, has a large ^{49}Ti depletion and falls outside of the correlation shown by the other Z grains and mainstream grains. The same grain falls close to the mainstream correlation line on the other two plots. We do not have a ready explanation for its unusual $^{49}Ti/^{48}Ti$ ratio.

In the $\delta^{50}Ti/^{48}Ti$ vs $\delta^{46}Ti/^{48}Ti$ plots (graphs (c) in Fig. 9-1 and 9-2) the Z grain data points plot above the mainstream correlation line just as they plot to the right of the mainstream line in a Si 3-isotope plot (Fig. 7). The reason

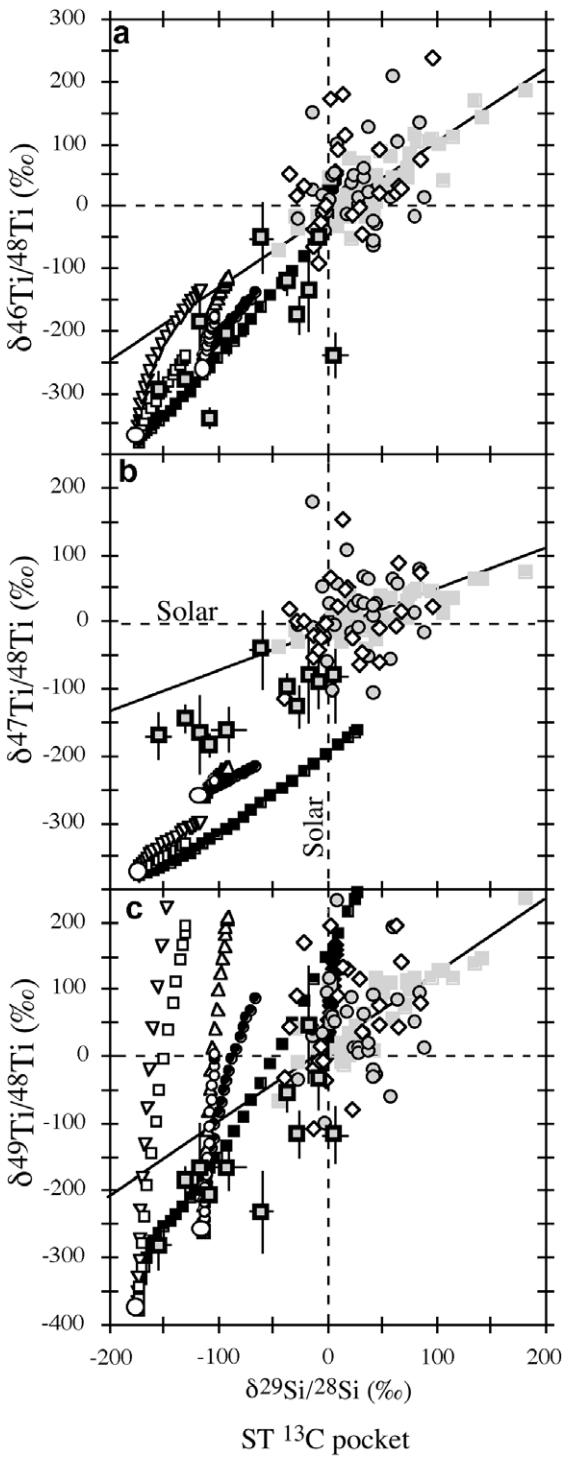

Fig. 10. Titanium isotopic ratios of presolar SiC grains are plotted against their $^{29}Si/^{28}Si$ ratios (in δ values). The solid lines are least-square fits to the isotopic ratios of mainstream grains. Also plotted are theoretical predictions for AGB stars and the ST ^{13}C pocket. The symbols for the grain data and the theoretical predictions are the same as those in Fig. 9. The grain data are from the same sources as in Fig. 9.

is that neutron-capture nucleosynthesis affects ^{50}Ti and ^{30}Si more than the other Ti and Si isotopes (Lugaro et al., 1999; Amari et al., 2001b; Zinner et al., 2006b), especially in low-metallicity stars (Table 5). Our assumed initial compositions and the GCE predictions by Timmes et al. (1995) plot above the mainstream correlation line. This discrepancy would be even larger if the correlation line is shifted down in order to take AGB nucleosynthesis into account for the mainstream grains as discussed above. However, there is more scatter in the $\delta^{50}Ti/^{48}Ti$ values than in the $\delta^{49}Ti/^{48}Ti$ and especially the $\delta^{47}Ti/^{48}Ti$ values. One reason is that the $^{50}Ti/^{48}Ti$ ratio is more susceptible to neutron capture in AGB stars. Another possible reason is that ^{50}Ti is produced in different stars than the other Ti isotopes. Whereas $^{46,47,48,49}Ti$ are mainly produced in Type II supernovae (Timmes et al., 1995; Woosley and Weaver, 1995; Rauscher et al., 2002), ^{50}Ti is mainly produced in Type Ia supernovae during deflagration of White Dwarf stars of masses near the Chandrasekhar limit (Meyer et al., 1996; Woosley, 1997). Such supernovae are very rare but produce large amounts of the neutron-rich isotopes of the Fe-peak elements. It is therefore expected that the distribution of ^{50}Ti in the ISM is more heterogeneous than that of the other Ti isotopes and the large ^{50}Ti excesses and deficits found in FUN and in refractory hibonite inclusions (Niederer et al., 1980; Fahey et al., 1987; Ireland, 1990; Sahijpal et al., 2000) are corroborating evidence. Thus, the larger scatter in the $^{50}Ti/^{48}Ti$ ratios of mainstream grains could originate from the heterogeneity of ^{50}Ti in the ISM. Type Ia supernovae become important in the later stages of GCE because White Dwarf stars are the end product of low- and intermediate-mass stars whose evolution takes much longer than that of massive stars, which explode as Type II supernovae. As a consequence, the GCE of ^{50}Ti is fundamentally different from those of the other Ti isotopes, which are secondary isotopes mostly produced in Type II supernovae (see Fig. 28 of Timmes et al., 1995), and our assumption that all Ti isotopes except ^{48}Ti evolve in the same way is not necessarily correct. A difference in the GCE of ^{46}Ti and ^{50}Ti as shown in the Timmes et al. figure means that the average Galactic evolutionary path in a $\delta^{50}Ti/^{48}Ti$ vs $\delta^{46}Ti/^{48}Ti$ 3-isotope plot is not a straight line but a curve that has a larger slope at low metallicity (at larger negative $\delta^{46}Ti$ values) than at close-to-solar metallicity.

In all three of the $\delta^{i}Ti/^{48}Ti$ vs $\delta^{29}Si/^{28}Si$ plots (Fig. 10) the Z grain data points extend the general trend exhibited by the mainstream grains but plot below the mainstream correlation line. This could mean that the GCE of the Ti isotopes differs from that of the Si isotopes in the earlier stages (low metallicity). However, in view of all the uncertainties, among them the correction for AGB nucleosynthesis, it is probably premature to make such a claim. As we did in Fig. 9-1 and 9-2 we plot theoretical predictions of AGB models in Fig. 10. In panel (a) the theoretical predictions are close to most Z grain data points, however, in panel (b) the predictions completely miss the grain data. This situation is similar to the one in panel (a) of Fig. 9-1 and 9-2 and must mean that the initial $^{47}Ti/^{48}Ti$ ratios we assumed for stars of low metallicity are too low. On purely mathematical grounds the disagreement between models and grain data in these two plots could also have been circumvented if we had assumed much lower initial $^{46}Ti/^{48}Ti$ and

Table 5
Final C, Ti and Si isotopic ratios from AGB models of different mass, metallicity, and ^{13}C pocket strength

Mass	Z	^{13}C pocket	Final C/O	Final ^{12}C/^{13}C	Final δ^{46}Ti	Final δ^{47}Ti	Final δ^{49}Ti	Final δ^{50}Ti	Final δ^{29}Si	Final δ^{30}Si
1.5	0.02	ST	1.15	42	29	6	75	135	3	15
		d3	1.15	42	15	3	62	59		
		d6	1.15	42	10	1	62	45		
		d12	1.15	42	8	0	64	37	3	13
	0.006	ST	4.96	313	−178	−237	2	537	−103	−55
		d3	4.96	313	−198	−243	−30	59	−103	−49
		d6	4.96	313	−216	−249	−51	−57	−102	−48
		d12	4.96	313	−229	−254	−59	−100	−102	−48
	0.003	ST	12.9	1170	−241	−332	195	1683	−130	86
		d3	12.9	1170	−240	−332	174	748	−127	109
		d6	12.9	1170	−264	−341	127	383	−126	120
		d12	12.9	1170	−288	−350	91	229	−125	126
2	0.02	ST	1.50	56	42	9	109	199	4	22
		d3	1.50	56	22	4	90	87		
		d6	1.50	56	15	2	88	67		
		d12	1.50	56	11	1	91	55	4	20
	0.006	ST	7.58	489	−114	−216	209	1315	−88	40
		d3	7.58	489	−149	−227	147	410	−86	54
		d6	7.58	489	−180	−237	106	181	−85	59
		d12	7.58	489	−203	−245	87	93	−84	60
	0.003	ST	20.6	2010	−138	−299	549	3742	−117	180
		d3	20.6	2010	−128	−296	531	1798	−103	272
		d6	20.6	2010	−176	−313	443	971	−101	291
		d12	20.6	2010	−228	−331	369	599	−98	304
3	0.02	ST	1.80	141	54	14	167	291	28	41
		d3	1.80	141	31	7	141	145		
		d6	1.80	141	22	4	138	119		
		d12	1.80	141	18	3	141	104	9	40
	0.006	ST	6.30	855	−140	−217	88	1126	−67	181
		d3	6.30	855	−151	−221	49	570	−66	198
		d6	6.30	855	−165	−226	20	411	−65	206
		d12	6.30	855	−175	−230	3	345	−64	213
	0.003	ST	17.4	4035	24	−160	245	2430	28	1531
		d3	17.4	4035	39	−150	276	2107	22	1530
		d6	17.4	4035	38	−151	265	1938	21	1536
		d12	17.4	4035	34	−153	253	1852	20	1543

^{29}Si/^{28}Si ratios. However, such a measure would create problems for other 3-isotope plots and higher initial ^{47}Ti/^{48}Ti ratios are the preferred solution. Panel (c) of Fig. 10 shows the same problem discussed above in connection with panel (b) of Fig. 9-1 and 9-2: most predicted shifts in the ^{49}Ti/^{48}Ti ratio are too large to be consistent with the grain data.

4.3.3. Inferred initial parent star compositions

As has previously been discussed (Alexander and Nittler, 1999; Amari et al., 2001b; Nittler and Alexander, 2003; Zinner et al., 2006b), the Si and Ti isotopic compositions of a given presolar SiC grain can be decomposed into two components, one reflecting the initial composition of the parent star, the other the effect of AGB nucleosynthesis. The parameters defined to express the parent star's initial composition are δ^{29}Si/^{28}Si$_{init}$ and δ^{46}Ti/^{48}Ti$_{init}$. They are obtained by projecting the isotopic composition of a given grain along theoretically predicted trajectories obtained from the AGB models onto the relevant assumed Galactic evolution line. The distance from this Galactic evolution line is the parameter expressing the effect of AGB nucleosynthesis and we express these shifts by Δ-values. This procedure is demonstrated for Si in Fig. 7 of Amari et al. (2001b) and Fig. 15 of Nittler and Alexander (2003). In this way we obtain the parameters Δ^{30}Si/^{28}Si and Δ^{50}Ti/^{48}Ti, which represent the isotopic shifts due to AGB nucleosynthesis. In principle, we can also obtain Δ^{47}Ti/^{48}Ti and Δ^{49}Ti/^{48}Ti but, as can be seen in Fig. 9-1 and 9-2, in the δ^{47}Ti/^{48}Ti vs δ^{46}Ti/^{48}Ti plot the predicted AGB trajectory

is approximately parallel to the mainstream correlation line and in the $\delta^{49}Ti/^{48}Ti$ vs $\delta^{46}Ti/^{48}Ti$ plot the data points do not deviate significantly from the correlation line.

We choose the mainstream correlation lines to represent the GCE lines. Equations for these lines as well as for the Si mainstream correlation line are given in Appendix A. As must be clear from the above discussion, this is only a rough approximation and the true GCE lines are shifted and probably have different slopes (steeper for $\delta^{49}Ti/^{48}Ti$ vs $\delta^{46}Ti/^{48}Ti$ and $\delta^{50}Ti/^{48}Ti$ vs $\delta^{46}Ti/^{48}Ti$). For the slope of the $\delta^{29}Si/^{28}Si$ vs $\delta^{30}Si/^{28}Si$ AGB trajectories we use 0.16, the average for the 1.5 and 2 $M_{\odot}$ models at $Z = 0.006$ and 0.003 if the Guber et al. (2003) neutron capture cross-sections are used (see Zinner et al., 2006b), for the $\delta^{50}Ti/^{48}Ti$ vs $\delta^{46}Ti/^{48}Ti$ trajectories we use 12.5, the average for the 1.5 $M_{\odot}$ models at $Z = 0.006$ and 0.003 for the ST ^{13}C pocket. Table 4 shows the $\Delta^{30}Si/^{28}Si$ and $\Delta^{50}Ti/^{48}Ti$ values that were obtained in this way for the Z grains and two Y grains from IH6. In Fig. 11 we plot the $\Delta^{50}Ti/^{48}Ti$ values against the $\Delta^{30}Si/^{28}Si$ values and find that they correlate with one another, although not perfectly. Because ^{50}Ti is much more affected by the ^{13}C source than is ^{30}Si, a perfect correlation is not necessarily expected. A least-squares-fit line through the data points has a positive intercept of the $\Delta^{50}Ti/^{48}Ti$ axis (Fig. 11). The reason for this intercept could be that the mainstream correlation line in the $\delta^{50}Ti/^{48}Ti$ vs $\delta^{46}Ti/^{48}Ti$ plot (graphs (c) in Fig. 9-1 and 9-2) does not represent the GCE line, which should be closer to the Z grain data points in this plot in order to result in a zero intercept of $\Delta^{50}Ti/^{48}Ti$ in Fig. 11. However, this is unlikely. Above we mentioned that, because of the effect of AGB nucleosynthesis in the parent stars of the mainstream grains, the GCE line should be shifted down rather than up from the mainstream correlation line and probably have a steeper slope. Furthermore, the predicted AGB trajectories for smaller ^{13}C pockets are shallower than those for the ST ^{13}C pocket (compare panels (panel (c) in Fig. 9-1 and 9-2) and a shallower slope for the trajectory lines would result in even larger $\Delta^{50}Ti/^{48}Ti$ values. At present, we do not have a ready explanation for this positive intercept.

In Fig. 12 we plot the initial $\delta^{46}Ti/^{48}Ti$ values of the grains' parent stars obtained by the deconvolution procedure against the initial $\delta^{29}Si/^{28}Si$ values. We do this for the Y and Z grains of this study, for the mainstream grains analyzed by Hoppe et al. (1994) and Alexander and Nittler (1999), and the Y grains analyzed by Amari et al. (2001b). Although there is considerable scatter, the data points exhibit a correlation between these two parameters, and the correlation line runs close to the origin. Thus, Fig. 12 expresses in a more elaborate, model-dependent, way the same fact as panel (a) in Fig. 10, namely a correlation between the $^{46}Ti/^{48}Ti$ and $^{29}Si/^{28}Si$ ratios. In Fig. 10 the ratios measured in the grains are plotted, while in Fig. 12 the inferred initial

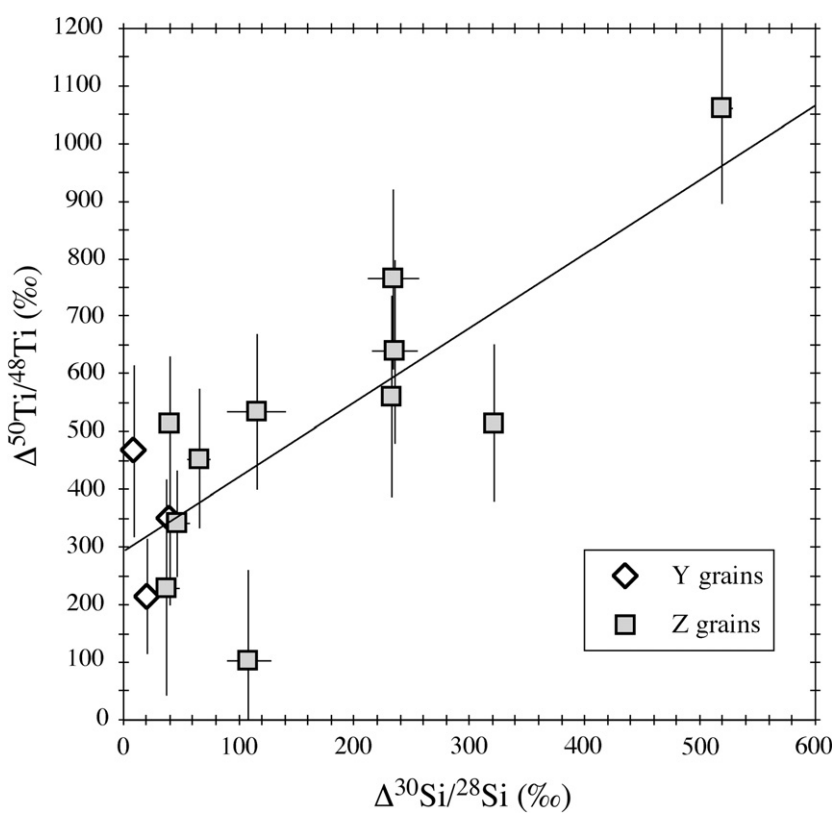

Fig. 11. Inferred isotopic shifts $\Delta^{50}Ti$ are plotted against $\Delta^{30}Si$ for Z grains and three Y grains from this study. The isotopic shifts are due to neutron-capture nucleosynthesis in AGB stars. They are obtained by projecting the Ti and Si isotopic ratios of the grains along lines predicted by theoretical models (the ST ^{13}C pocket) back onto the correlation lines for mainstream SiC grains. The solid line is a least-squares-fit line through the data points. See text for details.

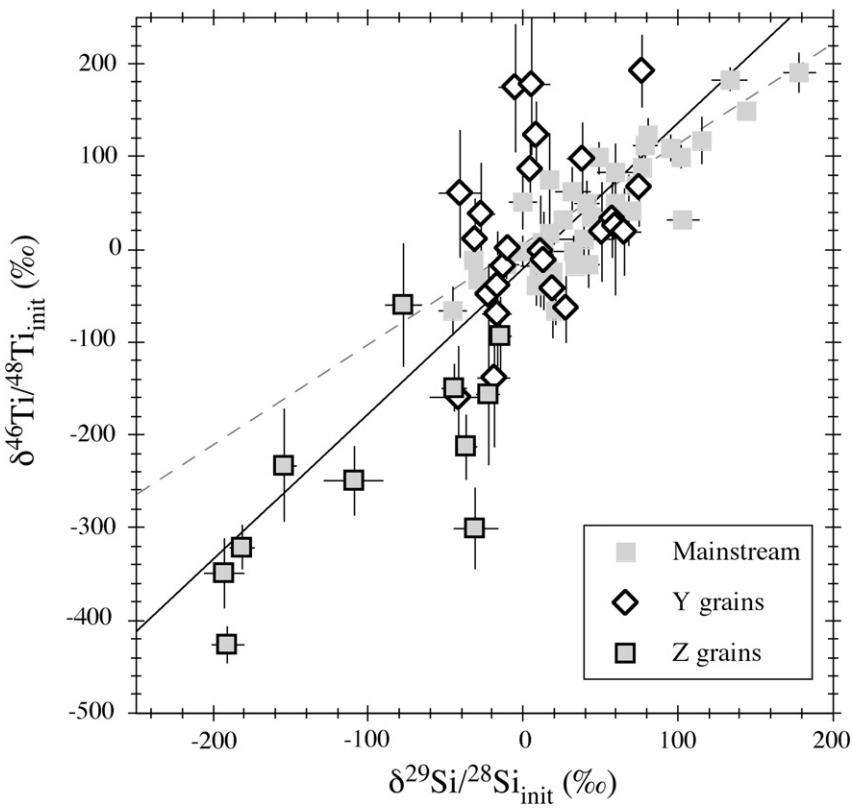

Fig. 12. Initial $\delta^{46}Ti/^{48}Ti$ values inferred from the $\delta^{50}Ti/^{48}Ti$ vs $\delta^{46}Ti/^{48}Ti$ plot ((c) in Fig. 9-1) are plotted against initial $\delta^{29}Si/^{28}Si$ values. These values, expressing the initial isotopic ratios of the grains' parent stars before they experienced any AGB nucleosynthesis, were obtained by projecting the Ti and Si isotopic ratios of the grains along lines predicted by theoretical models (the ST ^{13}C pocket) back onto the correlation lines for mainstream SiC grains. Plotted are values for the Z grains and three Y grains from this study, mainstream grains (This study, Hoppe et al., 1994; Alexander and Nittler, 1999), and Y grains (Amari et al., 2001b). The solid line is a least-squares-fit line through all the data points, the broken line is a fit through the mainstream grain data points. See text for details.

ratios of their parent stars are plotted. As in plot a of Fig. 10, most of the Z data grains plot below the correlation line of the mainstream grains (the broken line in Fig. 12).

In the same way as we obtained the initial $\delta^{46}Ti/^{48}Ti$ values from the $\delta^{50}Ti/^{48}Ti$ vs $\delta^{46}Ti/^{48}Ti$ plot (panel (c) in Fig. 9-1 and 9-2), we can obtain initial $\delta^{46}Ti/^{48}Ti$ values from the $\delta^{49}Ti/^{48}Ti$ vs $\delta^{46}Ti/^{48}Ti$ plot (panel (b) in Fig. 9-1 and 9-2). As a consistency check, Fig. 13-1 shows a plot of the two sets of $\delta^{46}Ti/^{48}Ti$ values for the ST ^{13}C pocket (Fig. 9-1). The solid line in this plot is not a best-fit line but the slope-one line through the origin, i.e., the line where for each grain the $\delta^{46}Ti/^{48}Ti$ values inferred in these different ways are equal. As can be seen, most data points plot close to this line, indicating that the GCE lines and AGB evolutionary trajectories are not too far from the correct ones. The alternative, that a shift in the CGE lines and a change in their slopes conspired in such a way as to produce the good agreement shown in Fig. 13-1, is unlikely but cannot be completely excluded. Fig. 13-2 shows a plot of the same initial $\delta^{46}Ti/^{48}Ti$ values but for the ST/6 ^{13}C pocket (Fig. 9-2). Because the AGB evolution lines for $\delta^{50}Ti/^{48}Ti$ vs $\delta^{46}Ti/^{48}Ti$ are less steep (we use a slope of 5.63, which is the average of the slopes for the 1.5 and 2 $M_{\odot}$ models for $Z = 0.006$ and 0.003) than for the ST pocket (average slope 12.5), these lines intercept the CGE line at lower $\delta^{46}Ti/^{48}Ti$ values and, as can be seen in Fig. 13-2, the data points for most Z grains and several Y grains plot below the slope-one line of equal initial $\delta^{46}Ti/^{48}Ti$ values.

Thus we arrive at contradictory conclusions from a comparison of the AGB models and the grain data. The slopes of the AGB evolutionary trajectories for the ST ^{13}C pocket gives a much better consistency between the initial $\delta^{46}Ti/^{48}Ti$ inferred from the $\delta^{49}Ti/^{48}Ti$ vs $\delta^{46}Ti/^{48}Ti$ plot and that inferred from the $\delta^{50}Ti/^{48}Ti$ vs $\delta^{46}Ti/^{48}Ti$ plot than for the ST/6 ^{13}C pocket (Fig. 13-1 and 13-2). However, the predicted shifts for the $^{49}Ti/^{48}Ti$ and $^{50}Ti/^{48}Ti$ ratios obtained with the ST pocket are much too large relative to the measured ratios in Z grains (panels (b) and (c) of Fig. 9-1) and are in better agreement for the ST/6 pocket (panels (b) and (c) of Fig. 9-2). A similar conclusion was reached by Huss and Smith (in press) on the basis of analysis of Ti isotopes in SiC grains from the Orgueil meteorite.

The Zr, Mo, and Ba isotopic ratios measured by RIMS in uncontaminated mainstream grains (Barzyk et al., submitted for publication) and the Ba ratios measured in the NanoSIMS (Marhas et al., in press) constrain the strength of the ^{13}C pocket to close to the ST case and none of these grains require a ^{13}C pocket of less than ST/2. At present we do not know whether this conclusion obtained for mainstream grains, i.e., grains originating from stars of solar

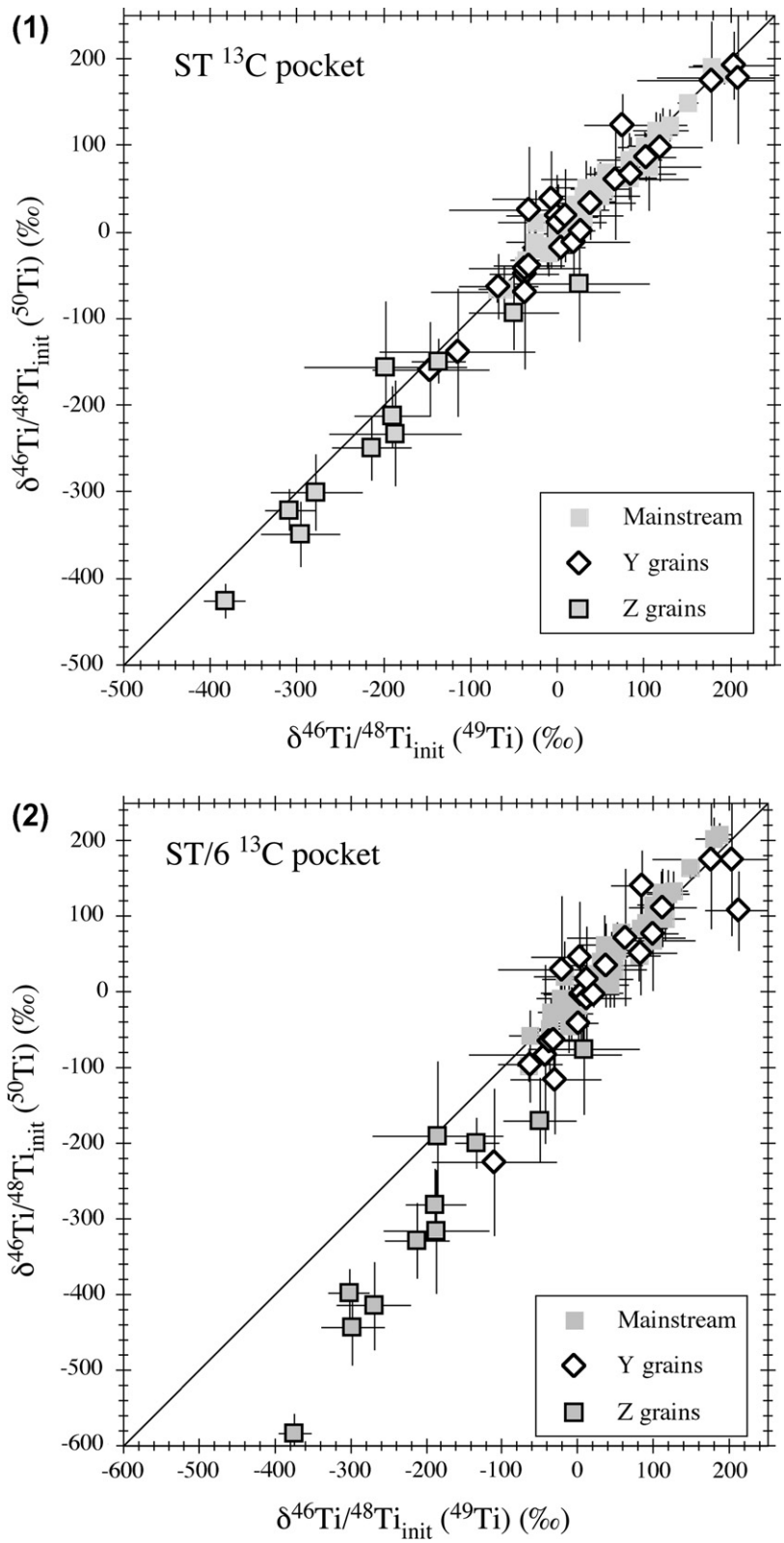

Fig. 13. (1) Initial $\delta^{46}Ti/^{48}Ti$ values inferred from the $\delta^{50}Ti/^{48}Ti$ vs $\delta^{46}Ti/^{48}Ti$ plot (panel (c) of Fig. 9-1) are plotted against initial $\delta^{46}Ti/^{48}Ti$ values inferred from the $\delta^{49}Ti/^{48}Ti$ vs $\delta^{46}Ti/^{48}Ti$ plot (panel (b) of Fig. 9-1). The slopes of the AGB evolution lines are for the ST ^{13}C pocket. Plotted are the same grains as those in Fig. 12. The solid line is a slope-one line through the origin. (2) The same as plot (1) but for the ST/6 ^{13}C pocket ((b) and (c) of Fig. 9-2). The data are from the same sources as for Fig. 12.

metallicity, also holds for all Z grains but RIMS analysis of one grain indicates that this is the case. This grain (with $\delta^{29}Si/^{28}Si = -125 \pm 13‰$ and $\delta^{30}Si/^{28}Si = 363 \pm 20‰$) has been analyzed for its Mo isotopic composition (Pellin et al., 2000). The measured ratios ($\delta^{92}Mo/^{96}Mo$, $\delta^{94}Mo/^{96}Mo$, $\delta^{100}Mo/^{96}Mo$) are consistent with the ST pocket, exclude any ^{13}C pocket strength of less than ST/2, and are completely inconsistent with ST/6.

Bonacic Marinovic et al. (in press) also modeled stars of lower-than-solar metallicity. Lead stars, which are very poor in metals at [Fe/H] < −2 need a ^{13}C pocket of ST/12 to cover the stellar populations. Halo stars with [Fe/H] ∼ −1 and Galactic post-AGB stars with at [Fe/H] > −1 seem to require the ST pocket. However, two post-AGB stars with [Fe/H] = −1 (Bonacic Marinovic et al., in press) and [Fe/H] = −1.4 (Reyniers et al., 2007) require a pocket of ∼ST/3.

There seems to be an indication that for low enough metallicities ^{13}C pocket strengths lower than ST are needed. However, we do not know at what metallicity this should happen and whether it applies for Z grains. If the parent stars of Z grains have a ST ^{13}C pocket, we would have to conclude that the predicted shifts in the $^{49}Ti/^{48}Ti$ and $^{50}Ti/^{48}Ti$ ratios in low-metallicity stars are too large and we have to look for possible reasons for this disagreement with the Z grain data. In a future paper, we will explore possible remedies to the models to bring them into better agreement with the grain data. These will include different assumptions for the initial Ti isotopic ratios of the parent stars and different assumptions for the Maxwellian averaged neutron capture cross-sections for the Ti isotopes.

5. SUMMARY AND CONCLUSIONS

We analyzed 463 SiC grains from Murchison and 154 SiC and 23 Si_3N_4 grains from Indarch for their C and N isotopic compositions, 549 SiC and 142 Si_3N_4 grains from Indarch for their C and Si isotopic compositions, 13 SiC grains from Murchison and 66 from Indarch for their Al–Mg compositions, and eight SiC grains from Murchison and 10 from Indarch for their Ti isotopic compositions. These measurements expanded the number of Al–Mg analyses on SiC Z grains from 4 to 23 and the number of Ti analyses on Z grains from 2 to 11. We also performed theoretical calculations to predict the C, Al, Si and Ti isotopic ratios in the envelope of AGB stars for different stellar masses and lower-than-solar metallicities. The grain analyses and the comparison with the theoretical models give the following results and conclusions:

1. Our measurements confirmed that the abundances of SiC grains of type Y and Z increase with decreasing grain size. The abundance of Z grains among SiC grains from Indarch separate IH6 (0.25–0.65 μm) is higher than any found before.
2. The enstatite chondrite Indarch contains Si_3N_4 grains. One of the ones we analyzed has the isotopic signatures of an X type grain. Although many of the others have isotopic anomalies in C, N, and Si, most of these anomalies can be explained to originate from adjacent presolar SiC grains. However, one grain with ^{13}C and ^{14}N excesses might have an AGB star origin.
3. The inferred $^{26}Al/^{27}Al$ ratios of Z grains are in the range found in mainstream and Y grains. Although cool bottom processing (CBP) has been invoked to explain the low $^{12}C/^{13}C$ ratios of Z grains, this process apparently does not lead to increased ^{26}Al production in the parent stars of these grains. This is in contrast to oxide grains where CBP is needed to explain their high $^{26}Al/^{27}Al$ ratios.
4. The low $^{46}Ti/^{48}Ti$, $^{47}Ti/^{48}Ti$, and $^{49}Ti/^{48}Ti$ ratios in Z grains and their correlation with low $^{29}Si/^{28}Si$ ratios extend the trend seen in mainstream grains and confirm an origin in low-metallicity AGB stars for this grain type.
5. The relative excesses in ^{30}Si and ^{50}Ti in Z grains are interpreted as being the result of increased production of these isotopes by neutron-capture nucleosynthesis in low-metallicity AGB stars. Such excesses are predicted by our AGB models. However, the predicted excesses in ^{50}Ti (and ^{49}Ti) greatly exceed those found in these grains and even lowering the strength of the ^{13}C pocket cannot solve this discrepancy in a consistent way. Future modeling efforts will hopefully lead to a resolution of this discrepancy.

ACKNOWLEDGMENTS

We thank Frank Stadermann for his expertise and discussions, Katharina Lodders for sharing her extensive knowledge on the condensation of grains in stellar environments, Tim Smolar and Elmar Gröner for their assistance with the NanoSIMS, and Frank Podosek for his support of Cristine Jennings. The detailed reviews by Uli Ott, Trevor Ireland, and an anonymous reviewer, as well as the comments by associate editor Sara Russell have helped in improving the manuscript. This work was supported by NASA Grants NNG05GF81G (E.Z., S.A., A.N.) and NNG04GF61G (L.R.N.), an Italian MIUR Grant (R.G.), and a NOW VENI Grant (M.L.).

APPENDIX A. MAINSTREAM CORRELATION LINES

Equations for the mainstream correlation lines were obtained from least-squares weighted fits to the data points with errors in both directions. They are for the Ti isotopes:

$$\delta^{47}Ti/^{48}Ti = (-10 \pm 2) + (0.54 \pm 0.04) \times \delta^{46}Ti/^{48}Ti$$

$$\delta^{49}Ti/^{48}Ti = (29 \pm 6) + (1.03 \pm 0.09) \times \delta^{46}Ti/^{48}Ti$$

$$\delta^{50}Ti/^{48}Ti = (43 \pm 12) + (1.94 \pm 0.18) \times \delta^{46}Ti/^{48}Ti$$

For the Si isotopes Hoppe et al. have given an equation for the mainstream correlation line:

$$\delta^{29}Si/^{28}Si = -15.7 + 1.34 \times \delta^{30}Si/^{28}Si$$

This equation has been updated several times (Lugaro et al., 1999; Nittler and Alexander, 2003). We have performed a new fit to mainstream grains with Si isotopic ratios listed in the database http://presolar.wustl.edu/~pgd/. From 6040 mainstream grains that had their Si isotopic

ratios measured we selected 4139 grains with $\delta^{29}Si/^{28}Si$ errors smaller and equal to 15‰ and $\delta^{30}Si/^{28}Si$ errors smaller than 25‰. For these grains we obtained the best-fit line

$$\delta^{29}Si/^{28}Si = (-19.9 \pm 0.6) + (1.37 \pm 0.01) \times \delta^{30}Si/^{28}Si.$$

REFERENCES

Abia C. and Isern J. (1997) $^{12}C/^{13}C$ ratios and Li abundances in C stars: evidence for deep mixing? *Mon. Not. R. Astron. Soc.* **289**, L11–L15.

Alexander C. M. O'D. (1993) Presolar SiC in chondrites: How variable and how many sources? *Geochim. Cosmochim. Acta* **57**, 2869–2888.

Alexander C. M. O'D. and Nittler L. R. (1999) The galactic evolution of Si, Ti, and O isotopic ratios. *Astrophys. J.* **519**, 222–235.

Alexander C. M. O'D., Swan P. and Prombo C. A. (1994) Occurrence and implications of silicon nitride in enstatite chondrites. *Meteoritics* **29**, 79–85.

Allende Prieto C., Lambert D. L. and Asplund M. (2001) The forbidden abundance of oxygen in the sun. *Astrophys. J.* **556**, L63–L66.

Allende Prieto C., Lambert D. L. and Asplund M. (2002) A reappraisal of the solar photospheric C/O ratio. *Astrophys. J.* **573**, L137–L140.

Amari S., Gao X., Nittler L. R., Zinner E., José J., Hernanz M. and Lewis R. S. (2001a) Presolar grains from novae. *Astrophys. J.* **551**, 1065–1072.

Amari S., Hoppe P., Zinner E. and Lewis R. S. (1995) Trace-element concentrations in single circumstellar silicon carbide grains from the Murchison meteorite. *Meteoritics* **30**, 679–693.

Amari S., Jennings C., Nguyen A., Stadermann F. J., Zinner E. and Lewis R. S. (2002) NanoSIMS isotopic analysis of small presolar SiC grains from the Murchison and Indarch meteorites. *Lunar Planet. Sci.* **XXXIII**. Abstract #1205.

Amari S., Lewis R. S. and Anders E. (1994) Interstellar grains in meteorites: I. Isolation of SiC, graphite, and diamond; size distributions of SiC and graphite. *Geochim. Cosmochim. Acta* **58**, 459–470.

Amari S., Nittler L. R., Zinner E., Gallino R., Lugaro M. and Lewis R. S. (2001b) Presolar SiC grains of type Y: Origin from low-metallicity asymptotic giant branch stars. *Astrophys. J.* **546**, 248–266.

Amari S., Nittler L. R., Zinner E., Lodders K. and Lewis R. S. (2001c) Presolar SiC grains of type A and B: Their isotopic compositions and stellar origins. *Astrophys. J.* **559**, 463–483.

Amari S., Zinner E., Gallino R., Lugaro M., Straniero O. and Domínguez I. (2005) Probing the Galactic chemical evolution of Si and Ti with presolar SiC grains. In *Origin of Matter and Evolution of the Galaxies 2003* (eds. M. Terasawa, S. Kubano, T. Kishida, T. Kajino, T. Motobayashi and K. Nomato). World Scientific, pp. 59–70.

Amari S., Zinner E. and Lewis R. S. (2000) Isotopic compositions of different presolar silicon carbide size fractions from the Murchison meteorite. *Meteorit. Planet. Sci.* **35**, 997–1014.

Anders E. and Grevesse N. (1989) Abundances of the elements: Meteoritic and solar. *Geochim. Cosmochim. Acta* **53**, 197–214.

Anders E. and Zinner E. (1993) Interstellar grains in primitive meteorites: Diamond, silicon carbide, and graphite. *Meteoritics* **28**, 490–514.

Angulo C., Arnould M., Rayet M., Descouvemont P., Baye D., Leclercq-Willain C., Coc A., Barhoumi S., Aguer P., Rolfs C., Kunz R., Hammer J. W. and Mayer A.The NACRE Collaboration (1999) A compilation of charged-particle induced thermonuclear reaction rates. *Nucl. Phys. A* **656**, 3–183.

Asplund M., Grevesse N. and Sauval A. J. (2005) The solar chemical composition. In *Cosmic Abundances as Records of Stellar Evolution and Nucleosynthesis, ASP Conference Series*, vol. 336 (eds. T. G. Barnes and F. N. Bash). Astronomical Society of the Pacific, San Francisco, pp. 25–38.

Bao Z. Y., Beer H., Käppeler F., Voss F., Wisshak K. and Rauscher T. (2000) Neutron cross sections for nucleosynthesis studies. *At. Data Nucl. Data Tables* **76**, 70–154.

Barzyk J. G., Savina M. R., Davis A. M., Gallino R., Gyngard F., Amari S., Zinner E., Pellin M. J., Lewis R. S. and Clayton R. N. (submitted for publication) Constraining ^{13}C amounts in AGB stars through measurement of trace elements in presolar SiC. *Meteorit. Planet. Sci.* **42**.

Bensby T., Feltzing S., Lundström I. and Ilyin I. (2005) α-, r-, and s-process element trends in the Galactic thin and thick disks. *Astron. Astrophys.* **433**, 185–203.

Bernatowicz T. J. and Zinner E. (eds.) (1997) *Astrophysical Implications of the Laboratory Study of Presolar Materials*. AIP, New York, p. 750.

Besmehn A. and Hoppe P. (2001) Silicon- and calcium-isotopic compositions of presolar silicon nitride grains from the Indarch enstatite chondrite. *Lunar Planet. Sci.* **XXXII**. Abstract #1188.

Besmehn A. and Hoppe P. (2003) A NanoSIMS study of Si- and Ca–Ti-isotopic compositions of presolar silicon carbide grains from supernovae. *Geochim. Cosmochim. Acta* **67**, 4693–4703.

Besmehn A., Mostefaoui S. and Hoppe P. (2001) Presolar minerals in the enstatite chondrite Sahara 97166. *Meteorit. Planet. Sci.* **36**, A20.

Bonacic Marinovic A. A., Izzard R.G., Lugaro M. and Pols O. R. (in press) The s-process in stellar population synthesis: a new approach in understanding AGB stars. *Astron. Astrophys.* **469**, 1013–1025.

Boothroyd A. I. and Sackmann I.-J. (1999) The CNO isotopes: deep circulation in red giants and first and second dredge-up. *Astrophys. J.* **510**, 232–250.

Boothroyd A. I., Sackmann I.-J. and Wasserburg G. J. (1994) Predictions of oxygen isotope ratios in stars and of oxygen-rich interstellar grains in meteorites. *Astrophys. J.* **430**, L77–L80.

Busso M., Gallino R. and Wasserburg G. J. (1999) Nucleosynthesis in asymptotic giant branch stars: relevance for Galactic enrichment and solar system formation. *Ann. Rev. Astron. Astrophys.* **37**, 239–309.

Chaplin W. J., Serenelli A. M., Basu S., Elsworth Y., New R. and Verner G. A. (submitted for publication) Solar heavy element abundance: constraints from frequency separation ratios of low-degree p modes. *Astrophys. J.*

Charbonnel C. (1995) A consistent explanation for $^{12}C/^{13}C$, ^{7}Li, and ^{3}He anomalies in red giant stars. *Astrophys. J.* **453**, L41–L44.

Choi B.-G., Huss G. R., Wasserburg G. J. and Gallino R. (1998) Presolar corundum and spinel in ordinary chondrites: Origins from AGB stars and a supernova. *Science* **282**, 1284–1289.

Choi B.-G., Wasserburg G. J. and Huss G. R. (1999) Circumstellar hibonite and corundum and nucleosynthesis in asymptotic giant branch stars. *Astrophys. J.* **522**, L133–L136.

Clayton D. D. and Nittler L. R. (2004) Astrophysics with presolar stardust. *Ann. Rev. Astron. Astrophys.* **42**, 39–78.

Clément D., Mutschke H., Kleinn R., Jäger C. and Dorschner J. (2005) Detection of silicon nitride particles in extreme carbon stars. *Astrophys. J.* **621**, 985–990.

Denissenkov P. A. and Tout C. A. (2003) Partial mixing and formation of the ^{13}C pocket by internal gravity waves in asymptotic giant branch stars. *Mon. Not. Roy. Astron. Soc.* **340**, 722–732.

Fahey A. J., Goswami J. N., McKeegan K. D. and Zinner E. (1987) ^{26}Al, ^{244}Pu, ^{50}Ti, REE, and trace element abundances in

hibonite grains from CM and CV meteorites. *Geochim. Cosmochim. Acta* **51**, 329–350.

Forestini M. and Charbonnel C. (1997) Nucleosynthesis of light elements inside thermally pulsing AGB stars: I. The case of intermediate-mass stars. *Astron. Astrophys. Suppl.* **123**, 241–272.

Forestini M., Paulus G. and Arnould M. (1991) On the production of ^{26}Al in AGB stars. *Astron. Astrophys.* **252**, 597–604.

Freytag B., Ludwig H.-G. and Steffen M. (1996) Hydrodynamical models of stellar convection—the role of overshoot in DA white dwarfs, A-type stars, and the Sun. *Astron. Astrophys.* **313**, 497–516.

Frost C. A. and Lattanzio J. C. (1996) AGB stars: what should be done? In *Stellar Evolution: What Should Be Done; 32nd Liège Int. Astroph. Coll.* (eds. A. Noel, D. Fraipont-Caro, M. Gabriel, N. Grevesse and P. Demarque). Université de Liège, Liège, Belgium, pp. 307–325.

Gallino R., Arlandini C., Busso M., Lugaro M., Travaglio C., Straniero O., Chieffi A. and Limongi M. (1998) Evolution and nucleosynthesis in low-mass asymptotic giant branch stars. II. Neutron capture and the s-process. *Astrophys. J.* **497**, 388–403.

Gallino R., Busso M. and Lugaro M. (1997) Neutron capture nucleosynthesis in AGB stars. In *Astrophysical Implications of the Laboratory Study of Presolar Materials* (eds. T. J. Bernatowicz and E. Zinner). AIP, New York, pp. 15–153.

Gao X., Nittler L. R., Swan P. D. and Walker R. M. (1995) Presolar grains in Indarch. *Meteoritics* **30**, 508.

Goriely S. and Mowlavi N. (2000) Neutron-capture nucleosynthesis in AGB stars. *Astron. Astrophys.* **362**, 599–614.

Guber K. H., Koehler P. E., Derrien H., Valentine T. E., Leal L. C., Sayer R. O. and Rauscher T. (2003) Neutron capture reaction rates for silicon and their impact on the origin of presolar mainstream SiC grains. *Phys. Rev. C* **67**, 062802-1–062802-5.

Heck P. R., Marhas K. K., Hoppe P., Gallino R., Baur H. and Wieler R. (2007) Presolar He and Ne isotopes in single circumstellar SiC grains. *Astrophys. J.* **656**, 1208–1222.

Herwig F. (2005) Evolution of asymptotic giant branch stars. *Ann. Rev. Astron. Astrophys.* **43**, 435–479.

Herwig F., Bloecker T., Schoenberner D. and El Eid M. (1997) Stellar evolution of low and intermediate-mass stars. IV. Hydrodynamically-based overshoot and nucleosynthesis in AGB stars. *Astron. Astrophys.* **324**, L81–L84.

Herwig F., Langer N. and Lugaro M. (2003) The s-Process in Rotating Asymptotic Giant Branch Stars. *Astrophys. J.* **593**, 1056–1073.

Hoppe P., Amari S., Zinner E., Ireland T. and Lewis R. S. (1994) Carbon, nitrogen, magnesium, silicon and titanium isotopic compositions of single interstellar silicon carbide grains from the Murchison carbonaceous chondrite. *Astrophys. J.* **430**, 870–890.

Hoppe P., Annen P., Strebel R., Eberhardt P., Gallino R., Lugaro M., Amari S. and Lewis R. S. (1997) Meteoritic silicon carbide grains with unusual Si-isotopic compositions: Evidence for an origin in low-mass low-metallicity asymptotic giant branch stars. *Astrophys. J.* **487**, L101–L104.

Hoppe P., Kocher T. A., Strebel R., Eberhardt P., Amari S. and Lewis R. S. (1996a) Origin of circumstellar SiC grains with low ^{12}C/^{13}C ratios: A multiple star scenario. *Lunar Planet. Sci.* **XXVII**, 561–562.

Hoppe P., Marhas K. K., Gallino R., Straniero O., Amari S. and Lewis R. S. (2004) Aluminum-26 in submicrometer-sized presolar SiC grains. *Lunar Planet. Sci.*. Abstract #1302.

Hoppe P. and Ott U. (1997) Mainstream silicon carbide grains from meteorites. In *Astrophysical Implications of the Laboratory Study of Presolar Materials* (eds. T. J. Bernatowicz and E. Zinner). AIP, New York, pp. 27–58.

Hoppe P., Strebel R., Eberhardt P., Amari S. and Lewis R. S. (1996b) Small SiC grains and a nitride grain of circumstellar origin from the Murchison meteorite: implications for stellar evolution and nucleosynthesis. *Geochim. Cosmochim. Acta* **60**, 883–907.

Hoppe P. and Zinner E. (2000) Presolar dust grains from meteorites and their stellar sources. *J. Geophys. Res.* **105**, 10371–10385.

Huss G. R., Hutcheon I. D. and Wasserburg G. J. (1997) Isotopic systematics of presolar silicon carbide from the Orgueil (CI) carbonaceous chondrite: Implications for solar system formation and stellar nucleosynthesis. *Geochim. Cosmochim. Acta* **61**, 5117–5148.

Huss G. R. and Smith J. B. (in press) Titanium isotopic compositions of well characterized silicon carbide grains from Orgueil (CI). *Meteorit. Planet. Sci.* **42**.

Iliadis C., D'Auria J. M., Starrfield S., Thompson W. J. and Wiescher M. (2001) Proton-induced thermonuclear reaction rates for $A = 20$–40 nuclei. *Astrophys. J. Suppl.* **134**, 151–171.

Ireland T. R. (1990) Presolar isotopic and chemical signatures in hibonite-bearing refractory inclusions from the Murchison carbonaceous chondrite. *Geochim. Cosmochim. Acta* **54**, 3219–3237.

Jennings C. L., Savina M. R., Messenger S., Amari S., Nichols, Jr., R. H., Pellin M. J. and Podosek F. A. (2002) Indarch SiC by TIMS, RIMS and NanoSIMS. *Lunar Planet. Sci.* **XXXIII**. Abstract #1883.

Karakas A. I. and Lattanzio J. C. (2003) Production of aluminium and the heavy magnesium isotopes in asymptotic giant branch stars. *Publ. Astron. Soc. Australia* **20**, 279–293.

Landi E., Feldman U. and Doschek G. A. (2007) Neon and oxygen absolute abundances in the solar corona. *Astrophys. J.* **659**, 743–749.

Lattanzio J. and Forestini M. (1999) Nucleosynthesis in AGB stars. In *Asymptotic Giant Branch Stars* (eds. T. Le Bertre, A. Lèbre and C. Waelkens). Astronomical Society of the Pacific, Provo, pp. 31–40.

Lattanzio J. C., Frost C. A., Cannon R. C. and Wood P. R. (1997) Hot bottom burning nucleosynthesis in 6 $M_\odot$ stellar models. *Nucl. Phys.* **A621**, 435c–438c.

Lattanzio J. C. and Lugaro M. A. (2005) What we do and do not know about the *s*-process in AGB stars. *Nucl. Phys. A* **758**, 477c–484c.

Lee M. R., Russell S. S., Arden J. W. and Pillinger C. T. (1992) The isotopic composition and mineralogy of silicon nitride (Si_3N_4) within ordinary and enstatite chondrites. *Meteoritics* **27**, 248–249.

Lin Y., Amari S. and Pravdivtseva O. (2002) Presolar grains from the Qingzhen (EH3) meteorite. *Astrophys. J.* **575**, 257–263.

Lodders K. and Amari S. (2005) Presolar grains from meteorites: remnants from the early times of the solar system. *Chem. Erde* **65**, 93–166.

Lugaro M., Davis A. M., Gallino R., Pellin M. J., Straniero O. and Käppeler F. (2003a) Isotopic compositions of strontium, zirconium, molybdenum, and barium in single presolar SiC grains and asymptotic giant branch stars. *Astrophys. J.* **593**, 486–508.

Lugaro M., Herwig F., Lattanzio J. C., Gallino R. and Straniero O. (2003b) s-Process nucleosynthesis in asymptotic giant branch stars: A test for stellar evolution. *Astrophys. J.* **586**, 1305–1319.

Lugaro M., Ugalde C., Karakas A. I., Görres J., Wiescher M., Lattanzio J. C. and Cannon R. C. (2004) Reaction rate uncertainties and the production of ^{19}F in asymptotic giant branch stars. *Astrophys. J.* **615**, 934–946.

Lugaro M., Zinner E., Gallino R. and Amari S. (1999) Si isotopic ratios in mainstream presolar SiC grains revisited. *Astrophys. J.* **527**, 369–394.

Marhas K. K., Hoppe P. and Ott U. (in press) NanoSIMS studies of Ba-isotopic compositions in presolar silicon carbide grains. *Meteorit. Planet. Sci.* **42**.

Meyer B. S., Krishnan T. D. and Clayton D. D. (1996) ^{48}Ca production in matter expanding from high temperature and density. *Astrophys. J.* **462**, 825–838.

Mowlavi N. and Meynet G. (2000) Aluminum 26 production in asymptotic giant branch stars. *Astron. Astrophys.* **361**, 959–976.

Nguyen A. N. and Zinner E. (2004) Discovery of ancient silicate stardust in a meteorite. *Science* **303**, 1496–1499.

Nichols, Jr., R. H., Kehm K. and Hohenberg C. M. (1995) Microanalytical laser extraction of noble gases: techniques and applications. In *Advances in Analytical Geochemistry*, vol. 2 (eds. M. Hyman and M. Rowe). JAI Press Inc., pp. 119–140.

Niederer F. R., Papanastassiou D. A. and Wasserburg G. J. (1980) Endemic isotopic anomalies in titanium. *Astrophys. J.* **240**, L73–L77.

Nittler L. R. (2003) Presolar stardust in meteorites: recent advances and scientific frontiers. *Earth Planet. Sci. Lett.* **209**, 259–273.

Nittler L. R. (2005) Constraints on heterogeneous galactic chemical evolution from meteoritic stardust. *Astrophys. J.* **618**, 281–296.

Nittler L. R. and Alexander C. M. O'D. (2003) Automated isotopic measurements of micron-sized dust: application to meteoritic presolar silicon carbide. *Geochim. Cosmochim. Acta* **67**, 4961–4980.

Nittler L. R., Alexander C. M. O'D., Gao X., Walker R. M. and Zinner E. (1997) Stellar sapphires: the properties and origins of presolar Al_2O_3 in meteorites. *Astrophys. J.* **483**, 475–495.

Nittler L. R., Alexander C. M. O'D., Stadermann F. J. and Zinner E. K. (2005a) Presolar Al-, Ca-, and Ti-rich oxide grains in the Krymka meteorite. *Lunar Planet. Sci.* **XXXVI**. Abstract #2200.

Nittler L. R., Gallino R., Lugaro M., Straniero O., Domínguez I. and Zinner E. (2005b) Si and C isotopes in presolar silicon carbide grains from AGB stars. *Nucl. Phys. A* **758**, 348c–351c.

Nittler L. R. and Hoppe P. (2004) New presolar silicon carbide grains with nova isotope signatures. *Lunar Planet. Sci.* **XXXV**. Abstract #1598.

Nittler L. R. and Hoppe P. (2005) Are presolar silicon carbide grains from novae actually from supernovae? *Astrophys. J.* **631**, L89–L92.

Nittler L. R., Hoppe P., Alexander C. M. O'D., Amari S., Eberhardt P., Gao X., Lewis R. S., Strebel R., Walker R. M. and Zinner E. (1995) Silicon nitride from supernovae. *Astrophys. J.* **453**, L25–L28.

Nollett K. M., Busso M. and Wasserburg G. J. (2003) Cool bottom processes on the thermally pulsing asymptotic giant branch and the isotopic composition of circumstellar dust grains. *Astrophys. J.* **582**, 1036–1058.

Ott U. (1993) Interstellar grains in meteorites. *Nature* **364**, 25–33.

Owen T., Mahaffy P. R., Niemann H. B., Atreya S. and Wong M. (2001) Protosolar nitrogen. *Astrophys. J.* **553**, L77–L79.

Pellin M. J., Davis A. M., Calaway W. F., Lewis R. S., Clayton R. N. and Amari S. (2000) Zr and Mo isotopic constraints on the origin of unusual types of presolar SiC grains. *Lunar Planet. Sci.* **XXXI**. Abstract #1934.

Piersanti L., Straniero O. and Cristallo S. (2007) A method to derive the absolute composition of the Sun, the solar system, and the stars. *Astron. Astrophys.* **462**, 1051–1062.

Rauscher T., Heger A., Hoffman R. D. and Woosley S. E. (2002) Nucleosynthesis in massive stars with improved nuclear and stellar physics. *Astrophys. J.* **576**, 323–348.

Reddy B. E., Tomkin J., Lambert D. L. and Allende Prieto C. (2003) The chemical compositions of Galactic disk F and G dwarfs. *Mon. Not. R. Astron. Soc.* **340**, 304–340.

Reimers D. (1975) Circumstellar envelopes and mass loss of red giant stars. In *Problems in stellar atmospheres and envelopes* (eds. B. Baschek, W. H. Kegel and G. Traving). Springer-Verlag, New York, pp. 229–256.

Reyniers M., Abia C., van Winckel H., Lloyd Evans T., Decin L., Eriksson K. and Pollard K. R. (2007) AGB nucleosynthesis in the Large Magellanic Cloud. Detailed abundance analysis of the RV Tauri star MACHO 47.2496.8. *Astron. Astrophys.* **461**, 641–650.

Russell S. S., Ott U., Alexander C. M. O'D., Zinner E. K., Arden J. W. and Pillinger C. T. (1997) Presolar silicon carbide from the Indarch (EH4) meteorite: comparison with silicon carbide populations from other meteorite classes. *Meteorit. Planet. Sci.* **32**, 719–732.

Sahijpal S., Goswami J. N. and Davis A. M. (2000) K, Mg, Ti and Ca isotopic compositions and refractory trace element abundances in hibonites from CM and CV meteorites: implications for early solar system processes. *Geochim. Cosmochim. Acta.* **64**, 1989–2005.

Savina M. R., Pellin M. J., Tripa C. E., Veryovkin I. V., Calaway W. F. and Davis A. M. (2003) Analyzing individual presolar grains with CHARISMA. *Geochim. Cosmochim. Acta* **67**, 3215–3225.

Siess L., Goriely S. and Langer N. (2004) Nucleosynthesis of s-elements in rotating AGB stars. *Astron. Astrophys.* **415**, 1089–1097.

Socas-Navarro H. and Norton A. A. (2007) The solar oxygen crisis: probably not the last word. *Astrophys. J.* **660**, L153–L156.

Stadermann F. J., Croat T. K., Bernatowicz T. J., Amari S., Messenger S., Walker R. M. and Zinner E. (2005) Supernova graphite in the NanoSIMS: Carbon, oxygen and titanium isotopic compositions of a spherule and its TiC sub-components. *Geochim. Cosmochim. Acta* **69**, 177–188.

Stone J., Hutcheon I. D., Epstein S. and Wasserburg G. J. (1991) Correlated Si isotope anomalies and large ^{13}C enrichments in a family of exotic SiC grains. *Earth Planet. Sci. Lett.* **107**, 570–581.

Straniero O., Chieffi A., Limongi M., Busso M., Gallino R. and Arlandini C. (1997) Evolution and nucleosynthesis in low-mass asymptotic giant branch stars. I. Formation of population I carbon stars. *Astrophys. J.* **478**, 332–339.

Straniero O., Domínguez I., Cristallo S. and Gallino R. (2003) Low-mass AGB stellar models for $0.003 \leqslant Z \leqslant 0.02$: basic formulae for nucleosynthesis calculations. *Publ. Astron. Soc. Australia* **20**, 389–392.

Straniero O., Gallino R. and Cristallo S. (2006) S process in low-mass asymptotic giant branch stars. *Nucl. Phys. A* **777**, 311–339.

Timmes F. X., Woosley S. E. and Weaver T. A. (1995) Galactic chemical evolution: Hydrogen through zinc. *Astrophys. J. Suppl.* **98**, 617–658.

Wasserburg G. J., Boothroyd A. I. and Sackmann I.-J. (1995) Deep circulation in red giant stars: a solution to the carbon and oxygen isotope puzzles? *Astrophys. J.* **447**, L37–L40.

Wasserburg G. J., Busso M., Gallino R. and Nollett K. M. (2006) Short-lived nuclei in the early Solar system: possible AGB sources. *Nucl. Phys. A* **777**, 5–69.

Woosley S. E. (1997) Neutron-rich nucleosynthesis in carbon deflagration supernovae. *Astrophys. J.* **476**, 801–810.

Woosley S. E. and Weaver T. A. (1995) The evolution and explosion of massive stars. II. Explosive hydrodynamics and nucleosynthesis. *Astrophys. J. Suppl.* **101**, 181–235.

Zinner E. (1998) Stellar nucleosynthesis and the isotopic composition of presolar grains from primitive meteorites. *Ann. Rev. Earth Planet. Sci.* **26**, 147–188.

Zinner E. (2004) Presolar grains. In *Meteorites, Planets, and Comets*, vol. 1 (ed. A. M. Davis), *Treatise on Geochemistry*, vol.

1 (eds. H. D. Holland and K. K. Turekian). Elsevier-Pergamon, Oxford, pp. 17–39.

Zinner E., Amari S., Guinness R. and Jennings C. (2003a) Si isotopic measurements of small SiC and Si_3N_4 grains from the Indarch (EH4) meteorite. *Meteorit. Planet. Sci.* **38**, A60.

Zinner E., Amari S., Guinness R., Nguyen A., Stadermann F., Walker R. M. and Lewis R. S. (2003b) Presolar spinel grains from the Murray and Murchison carbonaceous chondrites. *Geochim. Cosmochim. Acta* **67**, 5083–5095.

Zinner E., Amari S., Jennings C., Mertz A. F., Nguyen A. N., Nittler L. R., Hoppe P., Gallino R. and Lugaro M. (2005a) Al and Ti isotopic ratios of presolar SiC grains of type Z. *Lunar Planet. Sci.* **XXXVI**. Abstract #1691.

Zinner E., Nittler L. R., Alexander C. M. O'D. and Gallino R. (2006a) The study of radioisotopes in presolar dust grains. *New Astron. Rev.* **50**, 574–577.

Zinner E., Nittler L. R., Gallino R., Karakas A. I., Lugaro M., Straniero O. and Lattanzio J. C. (2006b) Silicon and carbon isotopic ratios in AGB stars: SiC grain data, models, and the Galactic evolution of the Si isotopes. *Astrophys. J.* **650**, 350–373.

Zinner E., Nittler L. R., Hoppe P., Gallino R., Straniero O. and Alexander C. M. O'D. (2005b) Oxygen, magnesium and chromium isotopic ratios of presolar spinel grains. *Geochim. Cosmochim. Acta* **69**, 4149–4165.

Associate editor: Sara S. Russell